Multi-walled carbon nanotube-induced genotoxic, inflammatory and pro-fibrotic responses in mice: Investigating the mechanisms of pulmonary carcinogenesis

Rahman, Luna; Jacobsen, Nicklas Raun; Aziz, Syed Abdul; Wu, Dongmei; Williams, Andrew; Yauk, Carole L.; White, Paul; Wallin, Hakan; Vogel, Ulla Birgitte; Halappanavar, Sabina

Published in:
Mutation research

Link to article, DOI:
10.1016/j.mrgentox.2017.08.005

Publication date:
2017

Document Version
Publisher's PDF, also known as Version of record

Mutat Res Gen Tox En 823 (2017) 28–44

Contents lists available at ScienceDirect

Mutat Res Gen Tox En

journal homepage: www.elsevier.com/locate/gentox

Multi-walled carbon nanotube-induced genotoxic, inflammatory and pro-fibrotic responses in mice: Investigating the mechanisms of pulmonary carcinogenesis

Luna Rahman[a], Nicklas Raun Jacobsen[b], Syed Abdul Aziz[c], Dongmei Wu[a], Andrew Williams[a], Carole L. Yauk[a], Paul White[a], Hakan Wallin[b,d], Ulla Vogel[b,e], Sabina Halappanavar[a,*]

[a] Environmental Health Science and Research Bureau, Health Canada, Ottawa, Canada
[b] The National Research Centre for the Working Environment, Copenhagen, Denmark
[c] Food Directorate, Health Products and Food Branch, Health Canada Ottawa, ON, Canada
[d] STAMI, National Institute of Occupational Health, Gydas vei 8, Oslo, Norway
[e] Department of Micro- and Nanotechnology, Technical University of Denmark, Lyngby, Denmark

ABSTRACT

The International Agency for Research on Cancer has classified one type of multi-walled carbon nanotubes (MWCNTs) as possibly carcinogenic to humans. However, the underlying mechanisms of MWCNT- induced carcinogenicity are not known. In this study, the genotoxic, mutagenic, inflammatory, and fibrotic potential of MWCNTs were investigated. Muta™Mouse adult females were exposed to 36 ± 6 or 109 ± 18 μg/mouse of Mitsui-7, or 26 ± 2 or 78 ± 5 μg/mouse of NM-401, once a week for four consecutive weeks *via* intratracheal instillations, alongside vehicle-treated controls. Samples were collected 90 days following the first exposure for measurement of DNA strand breaks, *lacZ* mutant frequency, p53 expression, cell proliferation, lung inflammation, histopathology, and changes in global gene expression. Both MWCNT types persisted in lung tissues 90 days post-exposure, and induced lung inflammation and fibrosis to similar extents. However, there was no evidence of DNA damage as measured by the comet assay following Mitsui-7 exposure, or increases in *lacZ* mutant frequency, for either MWCNTs. Increased p53 expression was observed in the fibrotic foci induced by both MWCNTs. Gene expression analysis revealed perturbations of a number of biological processes associated with cancer including cell death, cell proliferation, free radical scavenging, and others in both groups, with the largest response in NM-401-treated mice. The results suggest that if the two MWCNT types were capable of inducing DNA damage, strong adaptive responses mounted against the damage, resulting in efficient and timely elimination of damaged cells through cell death, may have prevented accumulation of DNA damage and mutations at the post-exposure time point investigated in the study. Thus, MWCNT-induced carcinogenesis may involve ongoing low levels of DNA damage in an environment of persisting fibres, chronic inflammation and tissue irritation, and parallel increases or decreases in the expression of genes involved in several pro-carcinogenic pathways.

1. Introduction

Multi-walled carbon nanotubes (MWCNTs) are increasingly incorporated into diverse manufactured products because of their high tensile strength, flexibility, adsorption capability, durability and light weight [1]. As a result, exposure to these materials in environmental and occupational settings, or *via* consumer products, is increasing. Variants of MWCNTs differ in wall numbers, wall thickness, fiber length, rigidity, and chemical impurities. The primary target organ for toxicological effects following exposure to MWCNTs is the lungs and uptake *via* the oral route is low [2,3]. Because of their size, MWCNTs have unrestricted access to most parts of the lung, can reach highly vascularised alveolar regions, interstitium and the pleural space, and exhibit a high degree of pulmonary biopersistence. In experimental animals, exposure to MWCNTs *via* inhalation, aspiration or intratracheal instillation [4–7] causes pulmonary inflammation, bronchiolar and alveolar hypertrophy, interstitial fibrosis, and granuloma formation [6–11].

* Corresponding author at: Environmental Health Science and Research Bureau, ERHSD, HECSB, Health Canada Tunney's Pasture Bldg. 8 (P/L 0803A), 50 Colombine Driveway, Ottawa, Ontario K1A 0K9 Canada.
E-mail address: sabina.halappanavar@hc-sc.gc.ca (S. Halappanavar).

http://dx.doi.org/10.1016/j.mrgentox.2017.08.005
Received 7 April 2017; Received in revised form 15 August 2017; Accepted 29 August 2017
Available online 08 September 2017

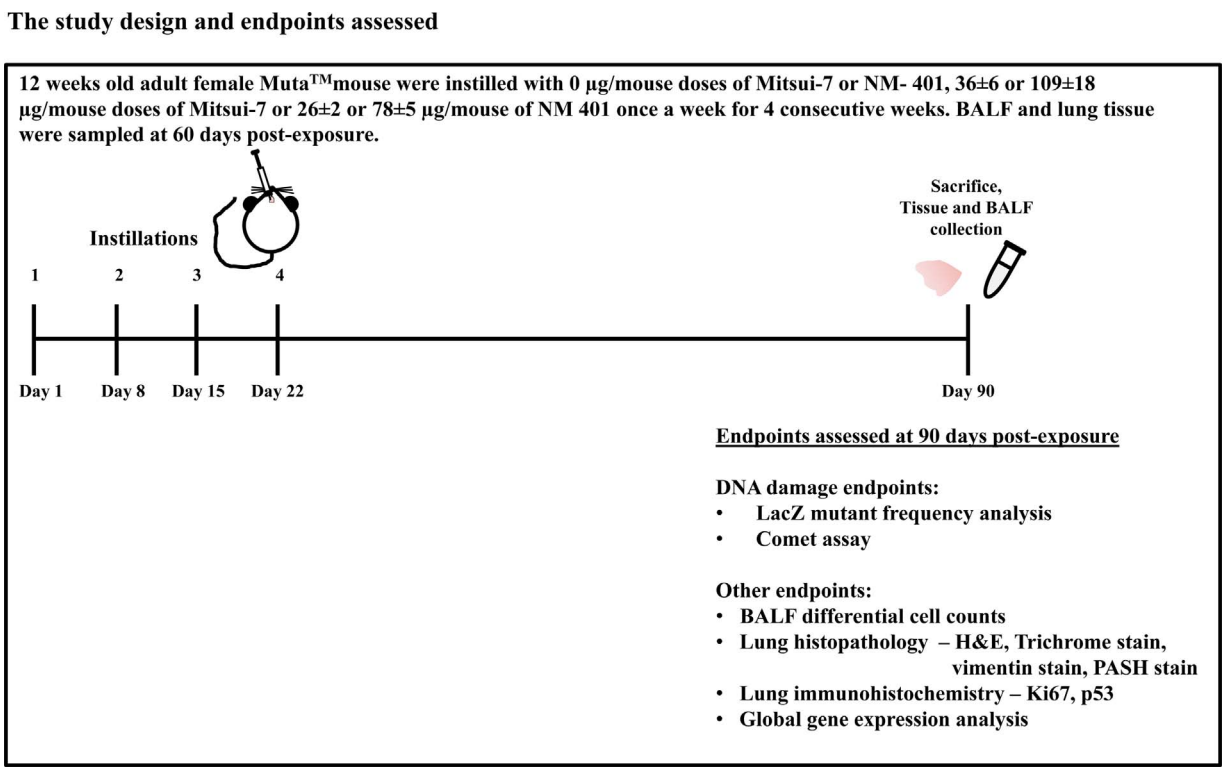

Fig. 1. Schematic diagram showing summary of experimental design.

Some studies have reported carcinogenic effects in abdominal cavities and bone marrow cells following intraperitoneal MWCNT exposure [12–16], and in the lungs of Imprinting Control Region mice following intratracheal instillation [17]. MWCNTs induce mesothelioma in tumor prone +/− P53 mice [14,15] and Fisher rats [13]. It is important to note that no data on human cancer following exposure to MWCNTs is available at present. A few studies have reported tumours in animal models exposed to Mitsui-7, a type of long straight MWCNTs at high doses. However, the results are inconsistent [18]. For other MWCNT types, data is not available. Based on the results of animal studies, the International Agency for Research on Cancer (IARC) has classified Mitsui-7 as possibly carcinogenic to humans (Group 2B) [19]. Indeed, Mitsui-7 was recently shown to induce lung cancer in a rat inhalation study [20]. Thus, there is some evidence that MWCNTs are carcinogenic. However, the underlying mechanisms are largely unknown and systematic research in this direction is urgently needed.

It has been suggested that thin and longer versions of MWCNTs induce cancer *via* mechanisms similar to other high-aspect ratio fibers such as asbestos. The mechanisms of toxicity associated with asbestos-induced cancer are attributed to specific fibre characteristics that include biopersistence, length, and rigidity [21]. Studies have shown that rigid MWCNTs such as Mitsui-7 exhibit a higher potential to induce cancer than the tangled MWCNTs [7,22,23]. Several *in vitro* studies [24–26] as well as *an in vivo* study [27] have shown that MWCNTs induce oxidative stress. Thus, oxidative damage of genetic material may be one mechanism by which MWCNTs initiate and/or promote cancer. However, a recent study by Sargent et al. (2014) showed that MWCNTs may not be directly carcinogenic; rather, it has been proposed that these materials act as promoters of murine pulmonary carcinogenesis [28].

Current models of carcinogenesis propose that substance-induced DNA damage, manifested *via* direct interaction of toxic substances or substance metabolite with DNA or indirect generation of DNA-damaging by reactive oxygen species (ROS) contributes to the formation of mutations, which can serve as initiating events in carcinogenesis. The accumulation of mutations in specific oncogenes or tumour suppressor genes, as well as successful selection and survival of cells harboring mutations, play important roles in inducing genetic instability and uncontrolled cellular proliferation, two important hallmarks of cancer [29]. However, it is not clear if DNA damage and resulting mutations play a role in the cancers induced by MWCNTs.

In addition to ROS generation and concomitant genotoxicity, MWCNTs induce both acute and chronic lung inflammation, which are also implicated in the etiology of substance-induced lung cancer [11]. Additionally, several studies have consistently demonstrated the potential of MWCNTs to induce lung fibrosis in experimental animals, which is also considered to be a precursor event to lung cancer in humans [30–32]. However, it is unknown if MWCNT-induced lung inflammation and fibrosis in experimental animals are indeed key events that lead to lung cancer. Moreover, the underlying mechanisms by which lung inflammation or lung fibrosis predispose organisms to carcinogenesis are not understood.

The study is based on two hypotheses – 1) CNTs are genotoxic and hence potentially carcinogenic, and 2) CNTs may induce carcinogenicity via non-genotoxic mechanisms that may involve lung inflammation and fibrotic injury. The specific objective of the study was to characterise the genotoxicity, mutagenicity, cellular proliferation, inflammatory and fibrosis effects in response to pulmonary MWCNT exposure in a mouse model with an aim to determine whether these are likely key events in the pathway leading to MWCNT-induced pulmonary carcinogenesis. The second objective was to identify the functional pathways and networks perturbed to understand the biology that is impacted and to characterise the molecular mechanisms at play. The study investigated two individual MWCNTs, Mitsui-7 and NM-401, both of which are straight and rigid fibres that exhibit similar physico-chemical properties. While Mitsui-7 has been categorised by IARC as possibly carcinogenic, the carcinogenic potential of NM-401 has not been investigated. To achieve the stated objectives, Muta™Mouse were exposed to vehicle only, Mitsui-7 or NM-401 (two doses per MWCNT type) once a week for four consecutive weeks *via* intratracheal instillations, and lungs, collected 90 days after the first instillation. Since pro-carcinogenic changes take time to establish, ninety days post-

Table 1
Characteristics of Mitsui-7 and NM-401.

MWCNT Code Name	Mitsui-7	NM-401
Producer	Mitsui' & Company	IO-LE-TEC Nanomaterials (CP-0006-SG)
MWCNT Code Name	Mitsui-7 (NRCWE-006)	NM-401
Tube diameter (TEM), nm	40–90[a],74[b], 49 − 100[c], 74 ± 28[e]	10–30[a], 67[b], 67 ± 26.2[d], 64.2 ± 34.5[e]
Tube length (TEM), μm	5.7 ± 0.49[b], 3–5[c], 5.7 ± 3.7[e]	5–15[a], 4.0 ± 0.37[b], 4.0 ± 2.4[d], 4.05 ± 2.4[e]
Straightness (TEM)	Straight	Straight
Surface area (BET), m^2/g	24–28[a],26[b], 22[e]	40–300[a],17.85[b], 18[e]
Surface area (SAXs), m^2/g		> 30
Impurities, %	< 1[a], < 0.5[c]	< 5[a], < 3[d]
Minor Impurity phases (XRD on TGA residual)[e]	Fe_2O_3	ND
SAXS aggregate size [nm][e]	NA	NA
DLS Zeta aggregate size [nm][e]	NA	NA
Minor elements (EDS)[e]	ND	Si: 500 ppm, Cu: 2300 ppm, Zn:
Minor elements/coatings (ICP-MS)[e]	Na, Mn, Al, Ni, Mg (Na: 499 ± 103 μg/g, Mg: 1 ± 1 μg/g, Al: 66 ± 19 μg/g, Fe: 355 ± 2 μg/g, Ni: 1 μg/g)	Na, Mn, Al, Ni, Mg (Na: 581 ± 32 μg/g, Fe: 379 ± 71 μg/g, Mg: 0 ± 0.3 μg/g, Al: 59 ± 4 μg/g, Ni: 2 μg/g)
Zeta-size and reactivity in 0.05% BSA water[e]		
DLS Zeta-size BSA medium [nm]	682 ± 13	710 ± 17
24-h dissolution	catalyst partially dissolved	catalyst partially dissolved
pH reactivity	negligible	(−)
dO_2 Reactivity	negligible	negligible
Rotating Drum Dustiness[e]		
Inhalable dustiness index	NA	NA
Respirable dustiness index	NA	NA

MWCNT: Multiwalled carbon nanotube; TEM: Transmission Electron Microscopy; BET: Brunauer–Emmett–Teller; SAXS: Small-Angle X-ray Scattering; DLS: Dynamic Light Sctattering; EDS: Energy-dispersive X-ray spectroscopy; ICP-MS: Inductively Coupled Plasma Mass Spectroscopy and BSA: Bovine Serum Albumin.
[a] Values claimed by manufacturer.
[b] Values reported by Jackson et al. [33].
[c] Values reported by Poulsen et al. [5].
[d] Values reported by Poulsen et al. [6].
[e] Values reported by NANOGENOTOX Final Report 2013.

exposure time point was chosen. The following endpoints were evaluated: (a) DNA damage assessed using the comet assay; (b) mutagenicity assessed by the *lacZ* transgene mutation assay; (c) inflammation assessed by bronchoalveolar lavage fluid (BALF) cell count; (d) histopathology and immunohistochemistry to measure cellular proliferation, fibrosis and p53 response; and (e) global changes in gene expression and pathophysiologic pathways. The experimental design, including the endpoints assessed, is summarized in Fig. 1.

2. Materials and methods

2.1. Properties of MWCNTs investigated

Two different MWCNTs were investigated in this study. The Mitsui XNRI-MWNT-7 (Mitsui-7; Lot# 05072001K28) was obtained from Mitsui Company (Tokyo, Japan) (now Hadoga Chemical Industry). NM-401 was a donation from the European Union Joint Research Centre, Ispra, Italy. NM-401 is also part of the OECD Working Party on Manufactured Nanomaterials testing program. The physico-chemical properties of Mitsui-7 [9,14,33] and NM-401 [6,33,34] have been published and are summarized in Table 1. Mitsui-7 exhibits tube diameters of 49–100 nm, and lengths of 3–5.7 μm; whereas NM-401 exhibits tube diameters of 30–90 nm, and lengths of 3.6–4.4 μm. The BET isotherm analysis showed surface areas of 22–26 m^2/g for Mitsui-7 and 17.85–18 m^2/g for NM-401. Inductively Coupled Plasma Mass Spectroscopy (ICP-MS) analysis showed that Mitsui -7 and NM-401 contain impurities such as iron (Fe), sodium (Na), aluminum (Al). Energy-dispersive X-ray spectroscopy (EDS) analysis showed that NM-401 also contains silica (Si), copper (Cu) and zinc (Zn).

2.1.1. Dose selection

Doses were selected based on the previously published studies on other nanoparticles [35,36]. Multiple instillations were chosen instead of a single instillation to increase the efficacy of the study. The total deposited doses are within the dose ranges used in other instillation or aspiration studies with carbon nanotubes [9,37–39], but are a physiologically high bolus dose in comparison to the NIOSH recommended occupational exposure limit of 1 $\mu g/m^3$ [40]. For mice, 45 years of work life exposure to 1 $\mu g/m^3$ for 40 h/week would result in 18 μg deposition with a deposition rate of 10% [41]. On the other hand, work place measurements of CNTs have been shown to be up to hundreds of times above the recommended exposure values [42–47]. Although, these are physiologically high doses, chronic inflammation and lung fibrosis has been observed in mice at these doses of Mitsui-7 and NM-401 [5,6]. Moreover, very high, 436 μg/mouse (Mitsui-7) and 312 μg/mouse (NM-401) doses were included in the study to determine if exposure to high doses of MWCNTs results in pulmonary genotoxicity and mutagenicity, as well as to conduct dose-response assessment of relevant endpoints. We have previously demonstrated that intratracheal instillation results in widespread delivery of material in murine lung [48], and that intratracheal instillation of serum dispersed MWCNTs results in delivery of MWCNTs to all lung lobes in mice [7].

2.1.2. Preparation of MWCNT stock and determination of exposure dose

A stock suspension of each MWCNT type was prepared fresh on the day of exposure at a concentration of 3.2 mg/mL in NanoPure water containing 2% serum collected from Muta™Mouse. The particle suspension was dispersed by sonicating the samples using an S-450D sonifier (Branson Ultrasonics Corp., Danbury, CT, USA) at 10% amplitude for a total of 16 min on ice with alternating 10 s pulses and pauses. Sonicated suspensions were diluted to the desired concentrations and sonicated for an additional 1 min with the same setting before their administration.

During the stock suspension preparation, it was noted that a fraction

of both types of MWCNTs remained unsuspended at the top of the particle suspension; this part was removed prior to exposure. In order to determine the exact exposure dose, the well-suspended portion was transferred to a new glass tube. Vehicle suspension that did not contain any MWCNTs was treated similarly. All suspensions were dried in an oven at 80 °C, and 50 µl vehicle or 1 ml particle suspensions were deposited on top of twenty-five mm glass microfiber filters grade GF-C (Whatman, Sigma-Aldrich) that were acclimatized to a controlled ambient environment for 24 h before being weighed on an ultra-fine analytical balance with 1 µg precision (XP6, Mettler Toledo). Following the deposition, the filters were incubated for 22 h at 80 °C and subsequently acclimatized for 24 h to ambient environment before being weighed.

The increase in filter weight deposited with vehicle-only suspension was subtracted from the filters treated with the MWCNT suspension. The exposure dose per 50 µl volume was then calculated from each instillation of the stock suspensions for all four weeks. For Mitsui-7 the doses were 36 ± 6 µg/mouse (low dose) and 109 ± 18 µg/mouse (high dose), and for NM-401 the doses were 26 ± 2 µg/mouse (low dose) and 78 ± 5 µg/mouse (high dose).

2.2. Animal handling and exposure

Adult 12 week old female Muta™Mouse were used in the study. The Muta™Mouse is a transgenic mouse (strain 40.6) with 29 ± 4 stably-integrated, concatenated copies of a non-transcribed λgt10*lac*Z shuttle vector [49,50] that contain a target transgene (i.e., *lac*Z) for determination of induced mutant frequency. The Muta™Mouse system has been employed to score induced *in vivo* mutations in over 30 tissues, and indeed, it has been used to assess the mutagenicity of over 300 test articles [51,52]. The mice are bred and maintained at Health Canada, Ottawa, Canada.

The mice were individually housed in plastic film isolators, provided with water and food *ad libitum* (2012 Teklad Global standard rodent diet), and maintained under a 12 h light/12 h dark cycle. The mice were randomly divided into five experimental groups consisting of 12 mice per group: 0 (i.e., control mice exposed to vehicle only, shared between the two particle types), 36 ± 6 or 26 ± 2 µg/mouse (i.e., low dose), and 109 ± 18 or 78 ± 5 µg/mouse (i.e., high dose) for Mitsui-7 and NM-401, respectively. Mice within each treatment group were exposed *via* intratracheal instillation once a week for four consecutive weeks. In a separate experiment, five additional mice per treatment group were exposed using the same treatment regimen with the sole purpose of collecting lung tissues for histopathological analyses.

The mice were anesthetized with 5% isofluorane until relaxed, and were kept under 2.5% isofluorane during the instillation process. During the entire procedure, the mice were held inclined at a 45 ° angle on their backs. Each instillation consisted of 50 µl MWCNT suspensions followed by 150 µl air, which was administered with a 250 µl SGE glass syringe (250F-LT-GT, SGE Analytical Science, Australia). Vehicle control exposure consisted of 50 µl 2% serum prepared in NanoPure water followed by 150 µl air. Following instillation, animals were kept under observation until recovery from anesthesia before moving them to their respective cages.

Ninety days following the first exposure the mice were anesthetized by isofluorane and sacrificed by cardiac puncture. Blood, BALF and lung tissues were collected. For transcriptomic analyses, lung tissues were collected after lavage. Post-lavage, the left and the right lobes of the lungs from exposed and control mice were cut into pieces, snap frozen in liquid nitrogen, and stored in cryogenic vials at −80 °C until analysis. All the analyses except transcriptomics were conducted in blind.

All animal procedures were conducted according to the guidelines for the care and handling of laboratory animals established by the Canadian Council for Animal Care Guidelines, and all protocols were approved by the Animal Care Committee of Health Canada.

2.3. Histopathology

For histopathological examinations, lung cross sections were prepared from 5 mice per treatment group (i.e., control, low dose, high dose) for each particle type. Lungs from control, Mitsui-7 or NM-401 exposed mice were uniformly inflated at 30 cm H_2O pressure with 10% formalin. Following 24 h of formalin fixation, lungs were dehydrated with graded alcohol, and paraffin embedded. 4-mm thick lung slices were cut. The resulting slides were stained with hematoxylin and eosin (H & E) to measure pathological changes and collagen deposition was assessed by Masson Trichrome stain. Images were acquired and analyzed using a Ziess-Axioskope-2 microscope (Carl Zeiss, Germany). A previously published guideline on International Harmonization of Nomenclature and Diagnostic Criteria (INHAND) was used to classify lung lesions [53]. Additionally, immunohistochemistry for the fibroblast marker vimentin, proliferation marker Ki67 and tumour suppressor p53 was also performed on formalin-fixed, paraffin embedded lung tissue sections. Ki67 and vimentin immuno-staining of lung sections was performed using kits, and according to the manufacturer's instruction (MACH 4 Universal HRP-Polymer Kit with DAB kit, Biocare Medical LLC, USA). Heat-induced epitope retrievals were performed at 110 °C for 12 min with citrate buffer (pH 6.0) prior to staining. In order to prevent endogenous peroxidases, 3% H_2O_2 was used. Incubations with primary Ki67 (BioCare Medical, Catalogue #CRM 325 A, 1:500 dilution) and Rabbit vimentin antibodies (Cell Signaling, Catalogue #5741, Clone D21H3, 1:100 dilutions) were conducted for 1 h at ambient temperature.

For detecting p53 expression, the Peroxidase Anti Peroxidase (PAP) technique was applied as described in previous studies [54,55]. Briefly, antigen retrieval was performed prior to staining by heating the lung sections in a microwave oven. Endogenous peroxidase activity and non-specific binding were blocked using 3% H_2O_2 in methanol and normal swine serum, respectively. The slides were incubated with monoclonal mouse anti-human p53 protein DO-7 (DAKO, Denmark) at 1:1000 dilution followed by incubation with rabbit anti-mouse immunoglobulin. Finally, the slides were treated with PAP complex and Di-aminobenzidine (DAB) before proceeding with imaging using a Perkin Elmer Vectra microscope (PerkinElmer, Waltham, MA).

Select sections were stained with Periodic acid Schiff-hematoxylin (PASH) to detect mucus production [56,57], Perls' Prussian blue containing 20% hydrochloric acid and 10% potassium ferrocyanide for 15 min, and nuclear fast red counter stain to detect iron homeostasis.

For quantification of fibrotic lesions, a series of images (using a 1.25x objective) of the entire longitudinal cross-section of the lungs from H & E stained lung sections were used. The disease area was defined by thickened alveolar septa, which also corresponded with areas of collagen deposition as determined by the Masson Trichrome staining. The disease area was traced and measured using Image J software (National Institute of Health, Bethesda, MD) and expressed as a percentage of the total cross-sectional area. Similarly, semi-quantitative analysis of Masson Trichrome and vimentin stain was conducted to determine the total collagen deposition and fibroblast proliferation in lungs, respectively. For Masson Trichrome and Vimentin, 5 individual images (using a 10x objective) were captured from each lung section from 5 mice.

2.4. Dark field and hyperspectral mapping of MWCNTs in lung sections

Haematoxylin and eosin stained lung sections were used for hyperspectral mapping of MWCNTs. Darkfield images of lung sections were captured at 100× magnification using a Cytoviva unit (Cytoviva, Inc., Auburn, AL) integrated onto an optical microscope. Hyperspectral images (HSI) were captured as previously described [36] using the HSI unit ENVI 4.8 software and mapped to the hyperspectral libraries for

the MWCNTs. The maximum acceptable angles between the known and unknown spectra were not greater than 0.1 rad.

In order to determine the orientation and localisation of MWCNTs within the lung tissue, 3D images of MWCNTs in lungs were captured. The Cytoviva Enhanced Dark Field Microscope equipped with a piezo-driven Z-axis stage, a dual mode fluorescence module, and Cytoviva's image acquisition and control software was used to acquire and store a stack of equally spaced images of the sample at 100× magnifications. At this magnification, the spatial resolution of the image pixel in the XY direction was 64.5 nm. Direct light from the dual mode fluorescence module was used to capture the images of the MWCNTs; light passing through a multi-pass filter was applied to capture the images of the surrounding tissue. The z resolution was set to 200 nm. The stack of images of the MWCNTs and the surrounding tissue were collapsed using the Cytoviva 3D Image Analysis Image J plugin *via* interpolation and deconvolution, respectively, in order to obtain 3D renderings. The 3D renderings were viewed with the 3D viewer in the Image J plugin.

2.5. Comet assay

DNA strand breaks were determined on frozen BALF cell suspensions and lung tissues (3 × 3 × 3 mm). Twelve mice from each group were lavaged twice with 1 ml of 0.9% sterile saline using an endotracheal tube with a 1 or 2 ml syringe to obtain BALF. The BALF was immediately put on ice until cells were separated by centrifugation at 4 °C and 400*g* for 10 min. The BALF cells were re-suspended in 0.5 ml PBS. Organ samples were snap frozen at dissection, and kept at −80 °C to −60 °C until analysis. The nucleoid preparation and automated comet analysis has previously been described in detail [58]. Briefly, frozen tissues were repeatedly pressed through a stainless steel cylindrical sieve (diameter 0.5 cm, mesh size 0.4 mm) into 1.5 ml ice-cold Merchant's medium. BAL cells and lung preparations were embedded in agarose (0.7% final concentration) and cast on TREVIGEN 20-well comet slides. These were immersed into 4 °C lysing solution and refrigerated overnight. The following day, samples were alkaline treated and subjected to alkaline electrophoresis (pH > 13) in ice cold circulating electrophoresis solution. Samples were neutralized, fixed, and later stained by SYBR Green. Comets were scored by the automated PathFinder system (IMSTAR, France). DNA strand breaks were quantified as the comet tail length (TL) and the% DNA in the comet tail (% tail DNA).

The comet experiment included eleven 20-well slides each of which included A549 cells as negative (treated with PBS for 30 min at 4 °C) and positive controls (treated with 60 mM H_2O_2 for 30 min at 4 °C). All slides with the same tissue were run in the same electrophoresis eliminating day-to-day or electrophoresis variation.

The variation in the results (% DNA in the tail and tail length) from the three control samples was 12–16% (negative control), 12–17% (positive control 30 and 60 mM).Statistical significance compared to control sample were determined by conducting non-parametric one-way ANOVA with a post- hoc Tukey-type analysis. A positive response was defined as a statistically significant increase in the% tail DNA in at least one dose group in comparison with the vehicle control.

2.6. LacZ mutant frequency analysis

Transgene (*lac*Z) mutant frequency was determined using the P-gal (phenyl-β-D-galactopyranoside) positive selection assay as described previously [7,51,52,59,60]. The λgt10*lac*Z DNA was rescued from genomic DNA using the Transpack® packaging system (Agilent Technologies, Mississauga, Ontario). The packaged phage particles were mixed with host bacterium (*Escherichia coli lac*Z$^-$, *gal*E$^-$, *rec*A$^-$, pA-A119 with *gal*T and *gal*K), plated on minimal medium containing 0.3% (w/v) P-Gal, and incubated overnight at 37 °C. Total plaque-forming units (pfu) were measured on concurrent plates that did not contain P-Gal. Mutant frequency was expressed as the ratio of the number of mutant pfu to total pfu, as described previously [51]. Statistical significance compared to control sample were determined by conducting non-parametric one-way ANOVA with a post- hoc Tukey-type analysis.

2.7. BALF analysis

The BALF samples were prepared as described previously [61]. Cytospins were fixed with two sprays of Sheldon Cell Fix, air dried, and stained with hematoxylin and eosin (H and E). At least 500 cells were counted per cytospin to identify mononuclear cells, neutrophils, and lymphocytes using an optical microscope (Olympus BH2, Olympus Optical Company Ltd, Tokyo, Japan) according to standard morphology. Percentage of each cell component was calculated and multiplied by the total cell number to determine the number of each cell component.

A Two-way ANOVA was conducted for each BALF component (i.e., different cell types) to examine the effect of particle type and dose (Origin version 8, Northampton, MA). Pair-wise comparisons with Bonferroni correction were conducted when significant interactions were observed.

2.8. Total RNA extraction and purification

Total RNA was isolated from random sections of the left lungs (n = 5 per experimental group) using TRIzol reagent (Invitrogen, Carlsbad, CA, USA), and purified using RNeasy Plus Mini kits (Qiagen, Mississauga, ON, Canada) according to the manufacturer's instruction. Total RNA concentration was measured using a NanoDrop 2000 spectrophotometer (Thermo Fisher Scientific Inc., Wilmington, DE, USA), and RNA quality and integrity was assessed using an Agilent 2100 Bioanalyzer (Agilent Technologies, Mississauga, ON, Canada) according to the manufacturer's instruction. All samples had RNA integrity numbers above 7.0.

2.9. Microarray hybridization

Total RNA (250 ng) from individual mice (n = 5 per experimental or control group) and Universal Mouse Reference total RNA (UMRR) (Agilent Technologies, Mississauga, ON, Canada) were used to synthesize double-stranded cDNA. Cyanine-labelled cRNAs were synthesized from the cDNA using Quick Amp Labeling Kit (Agilent Technologies, Mississauga, ON, Canada) according to the manufacturer's instructions. cRNAs from control and MWCNT-treated samples were labelled with Cyanine 5-CTP, and reference cRNAs were labelled with Cyanine 3-CTP using a T7 RNA polymerase *in vitro* transcription kit (Agilent Technologies, Mississauga, ON, Canada) and purified using RNeasy Mini kits (Qiagen, Mississauga, ON, Canada). An equimolar amount of reference cRNA was mixed with each experimental cRNA sample and was hybridized to Agilent mouse 8 × 60 k oligonucleotide microarrays (Agilent Technologies Inc., Mississauga, ON, Canada) for 17 h in a hybridization chamber at 65 °C with a rotation speed of 10 rpm. Following hybridization, arrays were scanned on an Agilent G2505B scanner according to manufacturer's protocols. Gene expression data from the scanned images were extracted using Agilent Feature Extraction software version 9.5.3.1.

2.10. Statistical analysis of microarray data

A reference randomized block design was used to analyse gene expression microarray data. Data were normalized using LOcally WEighted Scatterplot Smoothing (LOWESS) regression modeling method and statistical significance of the differentially expressed genes was determined using MicroArray ANalysis Of VAriance (MAANOVA) [62] in R statistical software (http://www.r-project.org). The Fs statistic [63] was used to test the treatment effects compared to the control vehicle, and p-values were estimated by the permutation method using

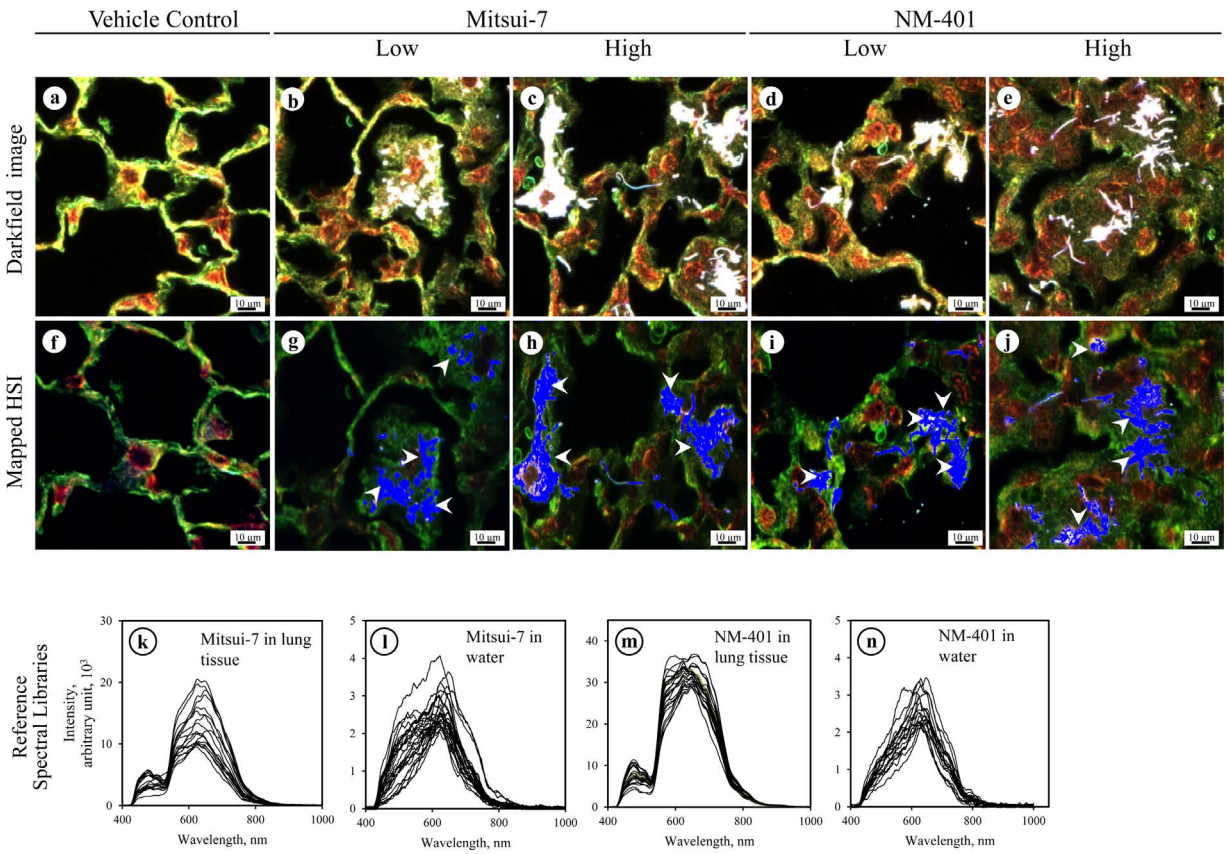

Fig. 2. Hyperspectral mapping of Mitsui -7 or NM-401 in lung tissue after 90 days of last exposure. The white arrows pointing towards the blue stained area represents MWCNTs.

residual shuffling. In order to minimize any false positives, the false discovery rate (FDR) multiple testing correction [64] was applied. The fold changes of gene expression were calculated considering the least-square means. Genes showing expression changes of at least 1.5-fold in either direction compared to their matched controls, and with FDR p-values of less than or equal to 0.05 ($p \leq 0.05$) were considered significantly differentially expressed, and were used in all downstream analyses. All microarray data have been deposited in the NCBI gene expression omnibus database and can be accessed *via* the accession number GSE75429.

2.11. Functional and pathway analysis of differentially expressed genes

Functional gene ontology (GO) analysis of the differentially expressed genes (DEGs) was performed using the Database for Annotation, Visualization and Integrated Discovery (DAVID) v6.7 [65]. Benjamini-Hochberg corrected GO processes with a Fisher's exact $p \leq 0.05$ were considered to be significantly enriched (i.e., over-represented). Specific biological pathways associated with the differentially expressed genes were identified using Ingenuity Pathway Analysis (IPA, Ingenuity Systems, Redwood City, CA, USA). Pathways with a Fisher's exact *p*-value ≤ 0.05 were considered for discussion.

3. Results

3.1. Physico-chemical properties of the MWCNTs used

The physico-chemical properties of Mitsui-7 [9,14,33] and NM-401 [6,33,34] are summarized in Table 1. The length and diameter of NM-401 used in the present study was characterised as part of European Union joint action NANOGENOTOX project. Mitsui-7 and NM-401 exhibit tube diameters of 74 ± 28 nm and 64.2 ± 34.5 nm, and lengths of 5.7 ± 3.7 μm and 4.05 ± 2.4 μm, respectively. The BET isotherm analysis showed surface areas of 22 m^2/g for Mitsui-7 and 18 m^2/g for NM-401. Thus, both MWCNT are relatively thick, long and have < 5% impurities.

3.2. Hyperspectral mapping of MWCNTs in lung sections

Hyperspectral mapping was conducted to determine whether Mitsui-7 or NM-401 persist in lung tissue 90 days post-exposure. In a hyperspectral image each pixel contains spectral information of that spatial pixel area. Thus, comparison between the tissue spectral profiles of hyperspectral images of Mitsui-7 or NM-401 in lung with the reference spectral libraries created for Mitsui-7 or NM-401 allowed localization and identification MWCNTs in lung. The darkfield images and corresponding mapped hyperspectral images of tissues exposed to vehicle only, Mitsui-7 or NM-401 at low and high doses are represented in Fig. 2a–e and in Fig. 2f–j, respectively. The areas of the hyperspectral images that matched to reference spectral libraries of Mitsui -7 or NM-401 in lung tissue are colored in blue and indicated by white arrow heads. The reference spectral libraries of Mitsui -7 or NM-401 in lung tissue, or as suspension in water, after background subtractions are represented in Fig. 2k–n. The hyperspectral mapping of MWCNTs revealed that notable amount of Mitsui-7 and NM-401 were retained in lung tissue even 90 days following the first exposure in both dose groups. Bimodal peaks were observed for the MWCNTs in the tissue matrix with predominant peaks at approximately 590 nm for Mitsui -7 (Fig. 2k) and 610 nm for NM-401 (Fig. 2m), and minor peaks at approximately 480 nm (Fig. 2k and m). Broader predominant peaks at approximately 550–650 nm were observed in the spectral libraries of Mitsui -7 or NM-401 as suspensions in water (Fig. 2l and n). Broad distributions of peak positions suggest non-homogeneities. The shifts in the peak positions between the reference spectral libraries and the MWCNT in the tissue matrix indicate changes in morphologies of these agglomerates as a result of interactions with tissue [66] over the 90 day

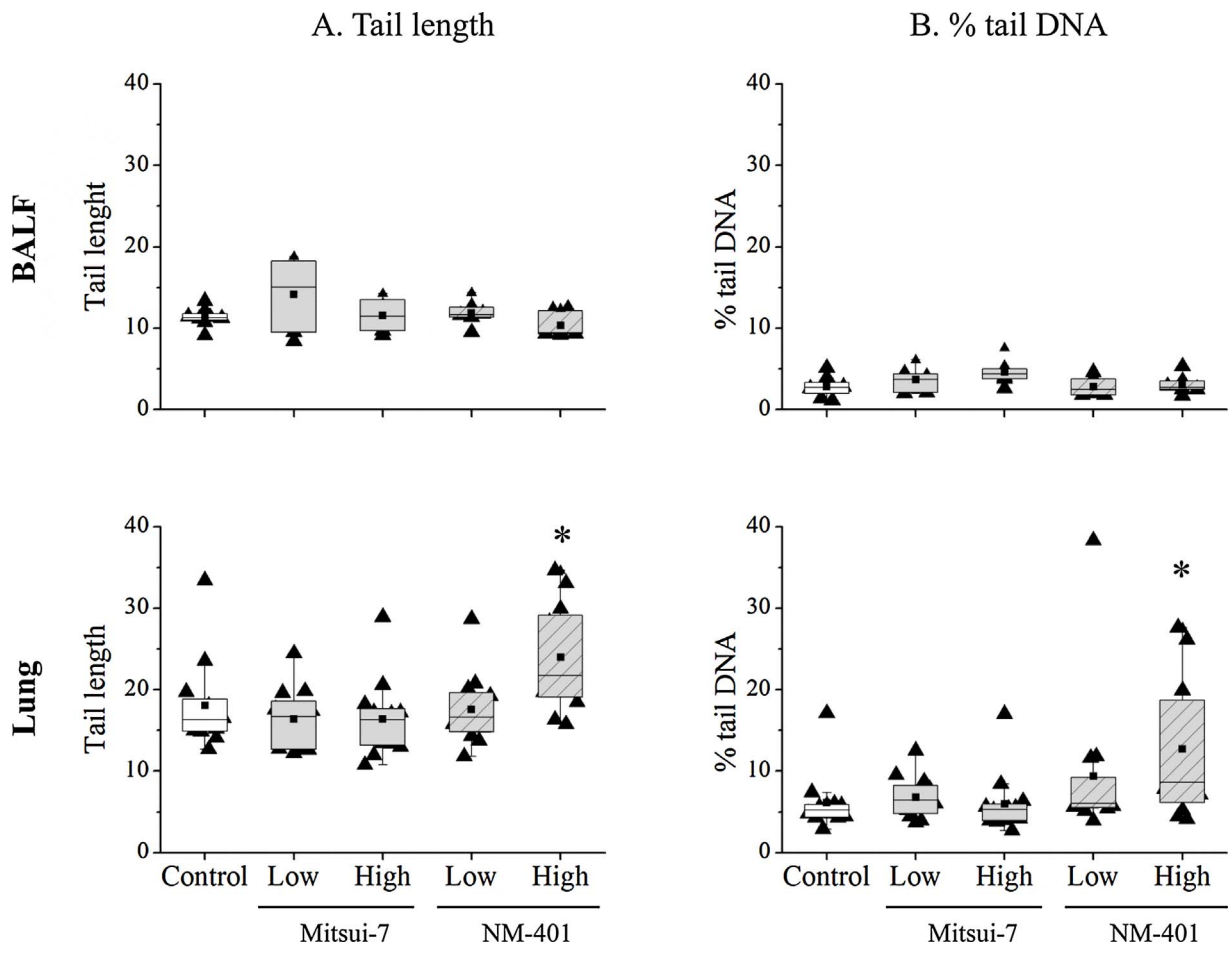

Fig. 3. DNA strand break levels determined using the Comet assay; (A) Tail length and (B) % tail DNA in BALF and in lung tissue from mice exposed to Mitsui -7 or NM-401 at low or high dose 90 days after last exposure. The statistical significance of the response in exposed group compared to matched vehicle controls was determined by a non-parametric one-way ANOVA with a post- hoc Tukey-type experimental comparison test. * indicates that the response is significantly different (p value ≤ 0.05) from the matched control.
The box plots illustrate median (black lines), mean (■), and data points (▲). *Statistically different from vehicle instilled mice at P ≤ 0.05. Box limits indicate the 75th nd 25th percentiles.

period. Visualization of the full rendering using 3D cytoviva (Supplementary movie 1) confirmed that the MWCNTs are in direct contact with the lung cells at the time of necropsy.

3.3. BALF and lung tissue genotoxicity and mutagenicity assessment

DNA damage was assessed in BALF and lung by quantifying DNA damage using the comet assay. The data, which are presented as tail length (TL) and tail% DNA, did not show any significant increase in DNA damage in the BALF of MWCNT-exposed mice relative to vehicle-exposed mice (Fig. 3, top panel). Similarly, no significant changes were observed in Mitsui-7-exposed lungs compared to matched controls. However, a significant increase in DNA strand breaks was observed in lungs of mice treated with high doses of NM-401 (Fig. 3, bottom panelb, Supplementary Table I) as measured by both comet parameters –TL and tail% DNA (18 ± 1.05 and 6.1 ± 1.63 versus 24 ± 2.42 and 12.7 ± 1.86 for high dose NM-401 and control, respectively). The errors here represent standard error mean.

Transgene (*lacZ*) mutant frequency (MF) analysis was used to determine the mutagenic potential of MWCNTs. Mean MF frequency for the control mice was $6.8 \pm 0.7 \times 10^{-5}$. Mice exposed to Mitsui-7 or NM-401 did not show statistically significant increases in the levels of transgene MF ($6.1 \pm 0.3 \times 10^{-5}$ or $6.4 \pm 0.5 \times 10^{-5}$, respectively) compared to control (Fig. 4) at any doses 90 days post-first exposure.

3.4. Cellular proliferation

Select lung tissue sections were analyzed for Ki-67 expression to examine the effects of MWCNT exposure on cell proliferation. Increased

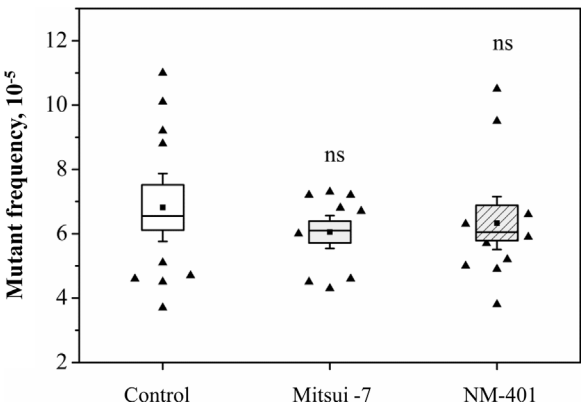

Fig. 4. Transgene *lacZ* mutation frequency in lung tissues from animals exposed to Mitsui -7 or NM-401 at low or high dose after 90 days of last exposure. The statistical significance of the response in exposed group compared to matched vehicle controls was determined by a non-parametric one-way ANOVA with a post- hoc Tukey-type experimental comparison test. NS – not significantly different from vehicle control. The box plots illustrate median (black lines), mean (■), and data points (▲).Box limits indicate the 75th nd 25th percentiles.

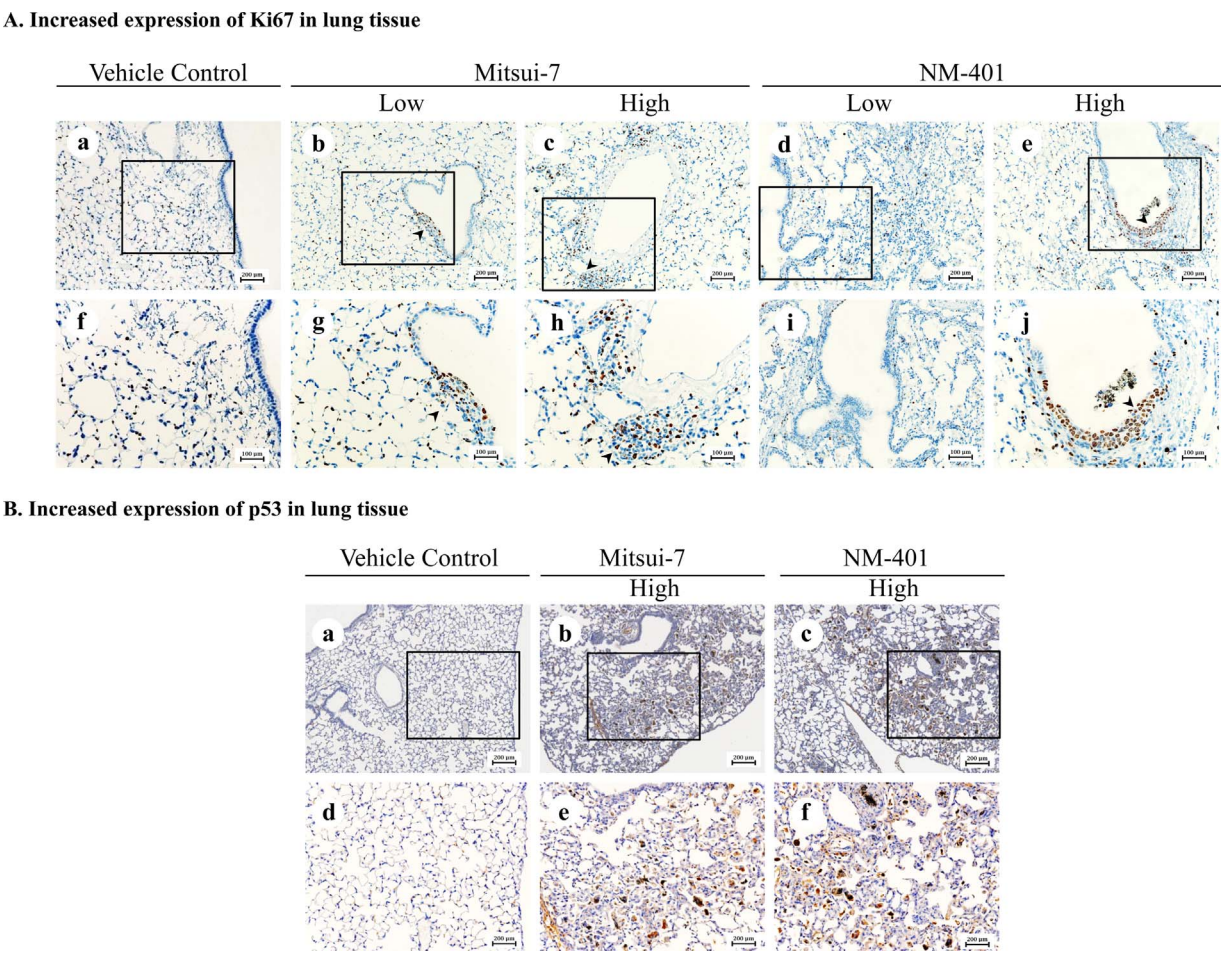

Fig. 5. Immunohistochemical detection of Ki67 (a–e, at 10× magnification and f-j at 20 x magnification) in lung tissues from animals exposed to Mitsui -7 or NM-401 at low or high dose, 90 days after the last exposure. Dark brown nuclear staining indicates increased levels of Ki67 expression. Arrowheads show area of elevated cellular proliferation, (arrowhead). (B) Immunohistochemical detection of p53 (a–c, at 10× magnification and d-f at 20× magnification) in lung tissues from animals exposed to Mitsui -7 or NM-401 at low or high dose, 90 days after the last. Dark brown nuclear staining indicates increased levels of p53 expression.

cellular proliferation compared to the matched control was observed for the low dose (Fig. 5A–b, g) and the high dose (Fig. 5A–c, h) Mitsui-7 treated lung sections. Cellular proliferation induced by NM-401 was comparable to that of the matched controls (Fig. 5A–d, i) in the low dose group, but higher compared to the matched control in the high dose group (Fig. 5A–e, j). Increased staining for Ki-67 was observed mainly near the bronchiolar ducts in these dose group animals.

3.5. p53 expression

Expression of p53 was investigated only in the high dose groups. Increased p53 expression was observed in the lung sections exposed to high doses of Mitsui-7 (Fig. 5B–b, e) and NM-401 (Fig. 5B–c, f), compared with control lung tissue sections (Fig. 5B–a, d). The p53 staining was predominantly found in the areas of fibrotic lesions, and was comparatively higher in the NM-401 exposed group.

3.6. Lung inflammation and fibrosis

3.6.1. BALF cell count

BALF from eight mice for the control group and six mice for each of the exposed groups was assessed for differential inflammatory cell counts (Fig. 6 and supplementary Table II a–b). At 90 days post-exposure, the total number of cells was ~7- and ~4.6-fold higher in BALF from mice exposed to Mitsui-7 or NM-401, respectively, compared to the vehicle exposed mice (Fig. 6a). A similar trend was found for macrophages (Fig. 6b).

The cellular profile shown in Fig. 6c revealed an increase in the number of neutrophils following MWCNT exposure. Specifically, there was a 134- and 160-fold increase in neutrophils following exposure to low and high doses of Mitsui-7, respectively, and a 76- and 100-fold increase following exposure to low and high doses of NM-401, respectively, compared to matched controls (Supplementary Table IIb). The number of lymphocytes also increased by 67- and 60-fold following exposure to Mitsui-7, and by 12- and 20-fold following exposure to NM-401 at the low and high doses, respectively (Fig. 6d; Supplementary Table IIb).No significant difference was observed in the eosinophil counts for control and MWCNT-exposed samples (Fig. 6e). The total number of epithelial cells was 10- and 14-fold higher in low and high dose Mitsui-7 exposed groups, respectively, and 3- and 5-fold higher in low and high dose NM-401 exposed groups compared to their matched controls, respectively (Fig. 6f, Supplementary Table IIb). The trends between the BALF cellular profiles of mice exposed to Mitsui-7 or NM-401 were comparable except for the total neutrophil and epithelial cells.

3.6.2. Histopathology

In accordance with the hyperspectral mapping results, histopathological analysis of H-E stained MWCNT-exposed lung tissues showed that significant amounts of MWCNTs were still present (Fig. 7A a–e) in the lungs 90 days post-exposure. MWCNTs were frequently found in bundles mainly in the fibrotic foci. The granulomatous lesions in MWCNT-exposed group were dominated by macrophages. Lesions occurred mainly, but not exclusively, in the centriacinar areas (CA), or at

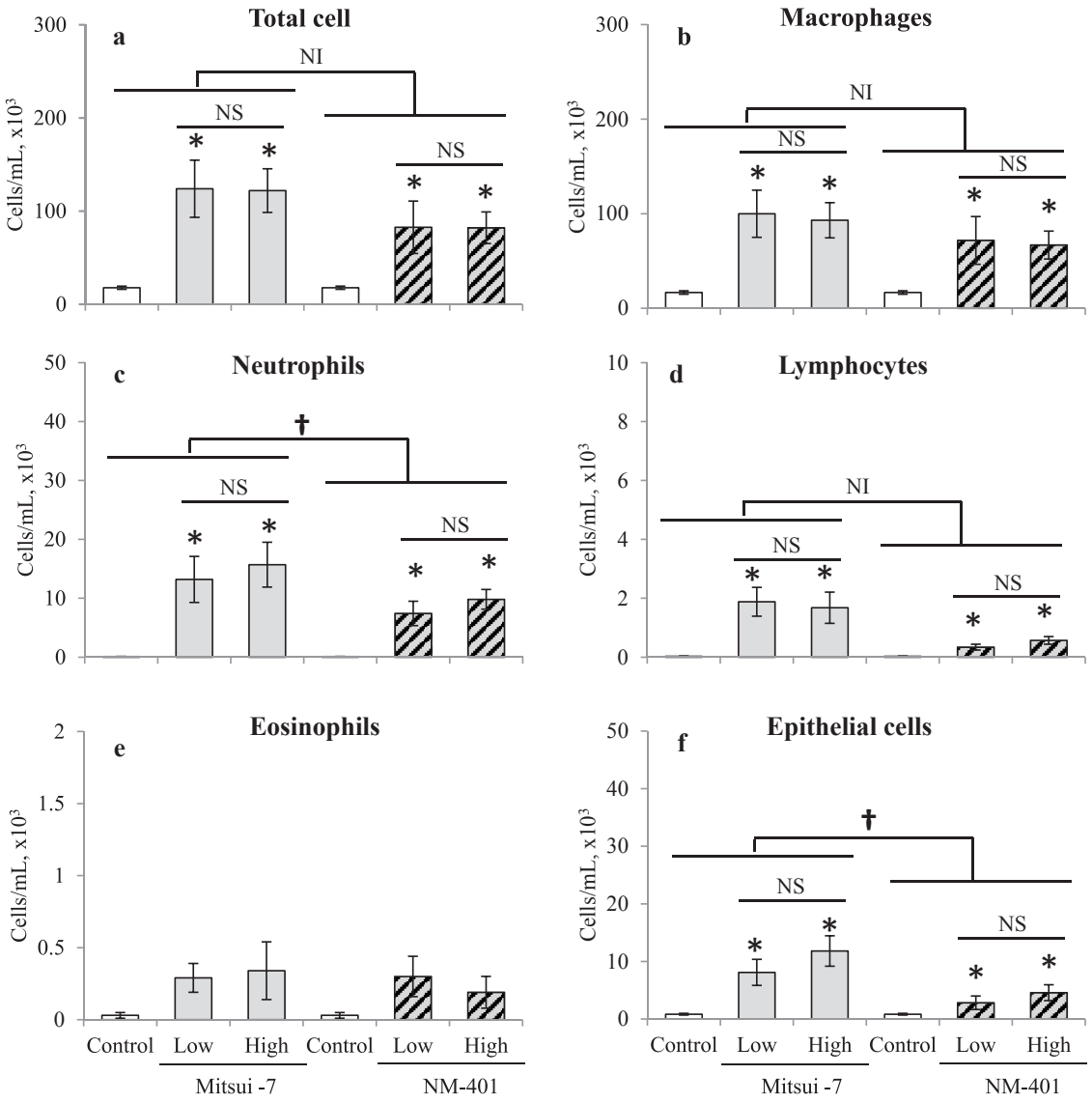

Fig. 6. Differential cell counts 90 days post-exposure in Bronchoalveolar Lavage Fluid (BALF) from animals exposed to vehicle control or Mitsui -7 or NM-401. The errors here represent standard error mean. * indicates that the response is significantly different at the 0.05 level. The response to each dose/MWCNT combination was determined by conducting two-Way-ANOVA. Post-hoc pair-wise comparisons, with the appropriate Bonferroni correction, were applied following a significant interaction to examine the effect of each dose/MWCNT combination. NI: no interaction between particle and dose main effects; †: significant interaction between dose and particle main effects; NS: non-significant.

the junctions of the terminal bronchioles and alveolar ducts (Fig. 7A a–e, Supplementary Table III). Quantification of the diseased area showed significant increase in disease area in MWCNT-exposed lungs compared to vehicle treated lungs from matched controls (Fig. 7A–a).

The lung sections were stained with Masson Trichrome stain (blue area) to assess collagen deposition, an indicator of fibrotic lesions. Minimal to mild collagen deposition (1.2% of the total area, 7B-b) was found in the vehicle treated lungs (Fig. 7A–f); more specifically, in the vascular and bronchiolar interstitium and the walls of the alveolar ducts. In the MWCNT-exposed mice, the amount of collagen was modestly increased to 2–2.6% (Fig. 7A g–j, 7B–b), with deposition in the walls or interstitium of alveolar ducts, alveoli, and airways. Mild collagen deposition was also observed in alveolar regions near the inflammatory cells and within the granulomas. Immunohistochemistry using an antibody against vimentin, a marker of fibroblasts, showed increased vimentin staining (1–1.2% of the total area (brown stain), Fig. 7B–c), in the MWCNT-exposed lung sections (Fig. 7A l–o); more specifically, in the areas of fibrosis in the high dose NM-401 group, which had the greatest vimentin staining (Fig. 7A–o). In contrast, vehicle treated controls (Fig. 7A–k) showed minimal vimentin staining (0.6% of the total area, 7B–c). Staining of lung sections with PAS, a marker for mucin production, showed increased mucin synthesis (black arrowheads) in the areas of airway epithelium (Supplementary Fig. 1a–e) in lungs exposed to both types of MWCNTs at all tested doses, relative to the vehicle exposed lungs. Additional staining for iron content using Prussian blue showed minimal staining of macrophages in lungs exposed to MWCNTs. One mouse showed significant increases in iron positive macrophages compared to vehicle-treated controls (Supplementary Fig. 1f–j).

3.6.3. *Gene expression analysis*

A list of DEGs (i.e., up- and downregulated genes) from samples collected 90 days post-exposure to Mitsui-7 or NM-401, relative to vehicle control, is presented in Supplementary Table IV. Fig. 8A summarizes the number of up- and downregulated genes for all dose-particle type combinations.

Mitsui-7 induced 1372 DEGs (i.e., 902 upregulated and 470 downregulated) and 1411 DEGs (i.e., 958 upregulated and 453 downregulated) in mouse lungs in the low and high dose groups, respectively. The largest expression changes were observed for members of

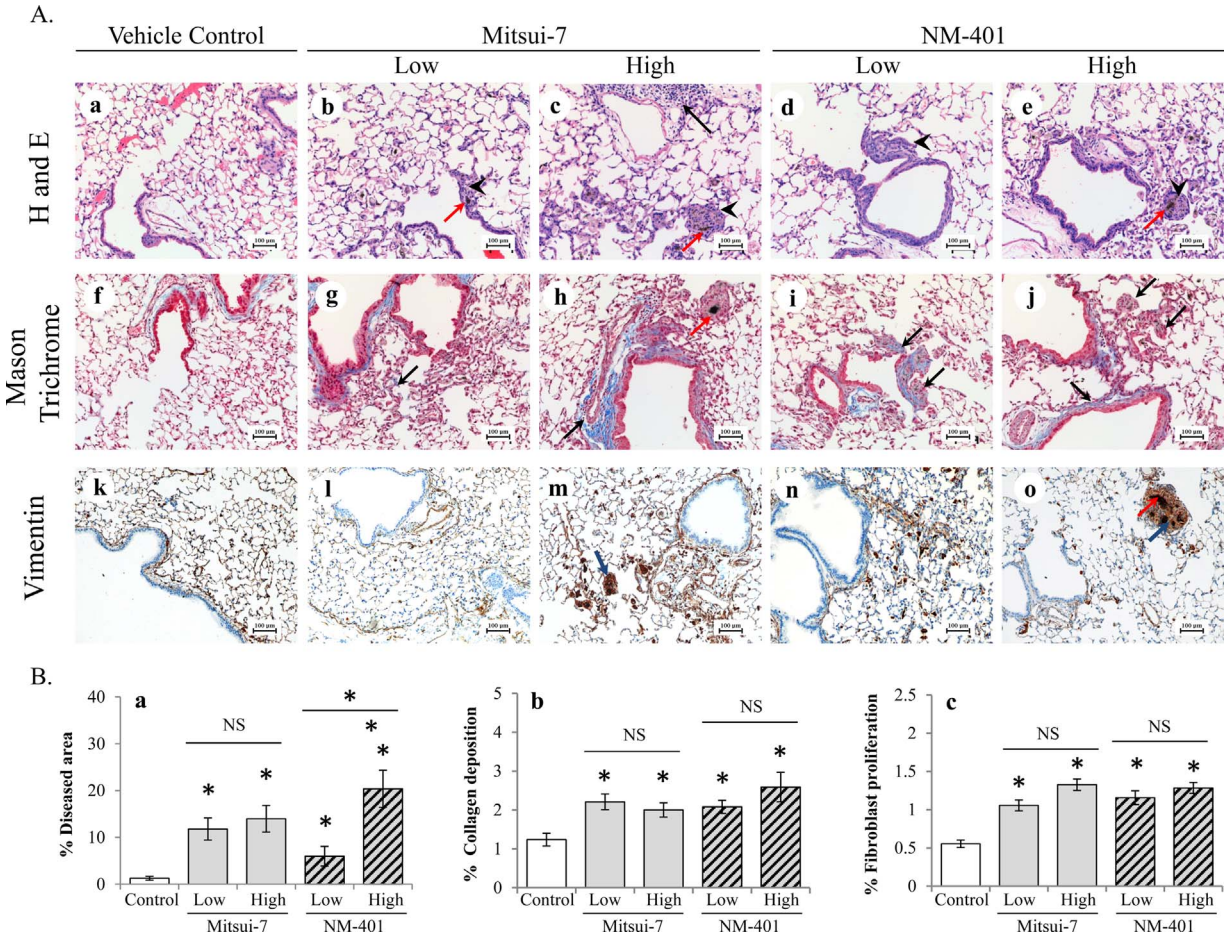

Fig. 7. (A) Histopathological images (10× magnification) of H and E, Mason Trichrome, and vimentin stained lung tissues from animals exposed to Mitsui -7 or NM-401 at low or high dose, 90 days after last exposure. The figures illustrate the presence of carbon nanotubes in tissue: red arrows (a–o), granuloma: black arrowhead (a–e), normal level of collagen deposition: blue coloured areas, increased level of collagen deposition: black arrows (f–j), and increased fibroblast proliferation: blue arrows (k–o). (B) Results of semi-quantitative analysis of the disease area (a), total collagen deposition (b), and total fibroblast proliferation (c). The response to MWCNT at each dose was compared to the matched control by two paired *t*-test. * indicates that the response is significantly different from the vehicle control (p value ≤0.05).

the chloride channel calcium activated 3 (*Clca3*, 172- and 153-fold increases for the low and high dose, respectively), chemokine (C-X-C motif) ligand 5 (*Cxcl5*, 8- and 4-fold), serum amyloid A 3 (*Saa3,* 25- and 19-fold), chemokine (C-C motif) ligand 7 (*Ccl7*, 13- and 10-fold), triggering receptor expressed on myeloid cells 2 (*Trem2*, 13- and 13-fold), glycoprotein (transmembrane) nmb (*Gpnmb*, 12- and 16-fold), *Spp1* (16- and 20-fold), lymphocyte antigen 6 complex, locus I, interferon (*Ly6i*, 8- and 6-fold), alpha-inducible protein 27 like 2A (*Ifi27l2a*, 6- and 4-fold), mucin 5, subtype B, tracheobronchial (*Muc5b*, 11- and 12-fold) and fibrinogen gamma chain (*Fgg*, 6- and 9-fold). There were 1073 DEGs (i.e., 731 up- and 342 downregulated) that were in common between the low and high dose groups (Fig. 8B–a) for both Mitsui 7 and NM-401, respectively.

The number of DEGs (1205) in the low dose NM-401 group was comparable to the low dose Mitsui-7 group (1372 DEGs) with 874 common DEGs between the two MWCNT groups (Fig. 8B–b). However, at the high dose, there was a large increase (214%, 2585 DEGs, 1459 upregulated and 1126 downregulated) in the number of DEGs in the NM-401 exposed lung samples compared to the high dose Mitsui-7 group (1411 DEGs). The largest expression changes compared to vehicle controls were observed for *Clca3* (62-, 177-fold), *Cxcl5*, (17- and 12-fold), *Saa3 (*17- and, 53-fold), *Ccl7* (11-, 25-fold), *Trem2* (11-, 25-fold), *Gpnmb* (10- and, 32-fold), *Spp1* (7- and 30-fold), *Ly6i* (9- and 8-fold), *Ifi27l2a* (9- and, 13-fold), *Muc5b* (9-, 13-fold) and *Fgg* (9- and 14-fold) genes in the low and high doses of NM-401, respectively. There were 978 DEGs (i.e., 679 up- and 299 downregulated) in common to dose groups of NM-401 (Fig. 8B–c). A total of 1199 DEGS (i.e., 781 up- and 418 downregulated) were affected by both MWCNTs in the high dose group (Fig. 8B–d).

Although the genes showing the largest expression changes for NM-401 were the same as the ones observed in the Mitsui-7 groups, the expression changes in the NM-401 exposed mice showed a clear dose-dependent response and exhibited larger fold changes than the Mitsui-7 group. However, the response was not dose-dependent for all genes, and higher expression was often observed in the low dose group compared to the high dose.

Enrichment analysis for GO terms showed that pulmonary exposure to Mitsui-7 and NM-401 induced perturbation in many biological processes (Fig. 9) at both doses including: immune response (GO:0006955), inflammatory response (GO:0006954), homeostatic process (GO:0042592), lymphocyte activation (GO:0046649), antigen processing and presentation (GO:0019882), cell adhesion (GO:0007155), myeloid leukocyte activation (GO:0002274), and cell proliferation (GO:0008283) (Fig. 9A). These biological processes are associated with inflammation and fibrosis. Biological processes enriched in Mitsui-7 or NM-401 exposed lungs at the high dose only included: acute inflammatory response (GO:0002526), regulation of cytokine production (GO:0001817), ion homeostasis (GO:0050801), skeletal system development (GO:0001501), epithelium development (GO:0060429), extracellular structure organization (GO:0043062), ossification (GO:0001503), regulation of cytoskeleton organization (GO:0051493), complement activation-classical pathway

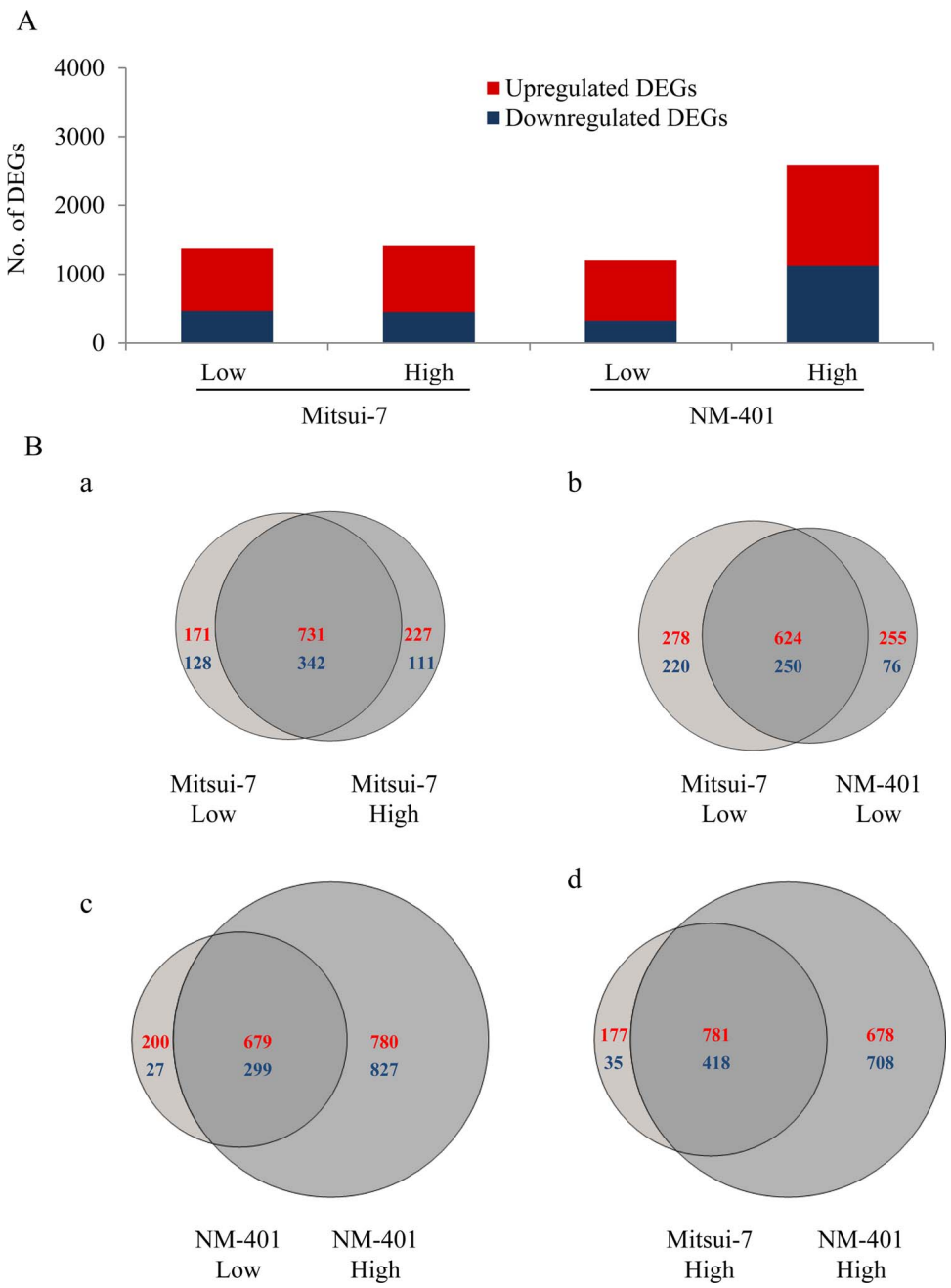

Fig. 8. (A) Significant differentially expressed genes (FDR p value ≤0.05) in lung tissues from animals exposed to Mitsui -7 or NM-401 at low or high dose, 90 days after the last exposure; (B) Venn diagram showing the comparisons between the numbers of DEGs at 90 days post-exposure in low and high dose groups of Mitsui -7 (a), low dose groups of Mitsui and NM-401 (b), low and high dose groups of NM-401 (c) and high dose groups of Mitsui -7 and NM-401 (d).

(GO:0006958), and cell death (GO:0008219) (Fig. 9B). In addition, biological processes associated with DNA damage (intracellular signaling cascade (GO:0007242), apoptosis (GO:0006915), angiogenesis (GO:0001525), regulation of MAPKKK cascade (GO:0043408), ATP metabolic process (GO:0046034), response to oxidative stress (GO:0006979), anti-apoptosis (GO:0006916) and regulation of DNA binding (GO:0051101)) were also perturbed in treated lungs at the high doses.

Global gene expression and ingenuity biological functions analysis revealed perturbations of a vast number of biological functions in response to both particle types. While inflammatory response and related functions were among those functions predominantly affected, other processes related to fibrosis (e.g., connective tissue disorders), cancer (e.g., cytotoxicity, cell viability, advanced malignant tumor, metastasis, and invasion of tumor), arthropathy and cardiovascular diseases, were also significantly (p-values $< 5 \times 10^{-8}$) impacted. The results of the pathway analysis showing the top impacted diseases and functions associated with the DEGs in lung samples exposed to Mitsui-7 or NM-401 at both doses are presented in Supplementary Fig. 2A. The number of DEGs associated with these pathways and functions was higher in lungs exposed to NM-401 than Mitsui-7.

In order to understand disease mechanisms, canonical pathways were analysed using IPA (Supplementary Fig. 2B). Most significantly perturbed pathways were associated with inflammation, hepatic fibrosis and oxidative damage, and genes in these pathways were enriched in both MWCNT groups. The number of genes and the fold changes of DEGs associated with the fibrosis and DNA damage pathways was higher in NM-401 than Mitsui-7 exposed mouse lungs.

Several upstream regulators had fold change values above 1.3, and the activation state and significance of a regulator were predicted from the Z-score calculated in IPA. An upstream regulator with a positive Z-score was considered to be potentially activated, whereas an upstream regulator with a negative Z-score was considered to be potentially inhibited. An upstream regulator with a Z-score ≥ 2 was considered to be

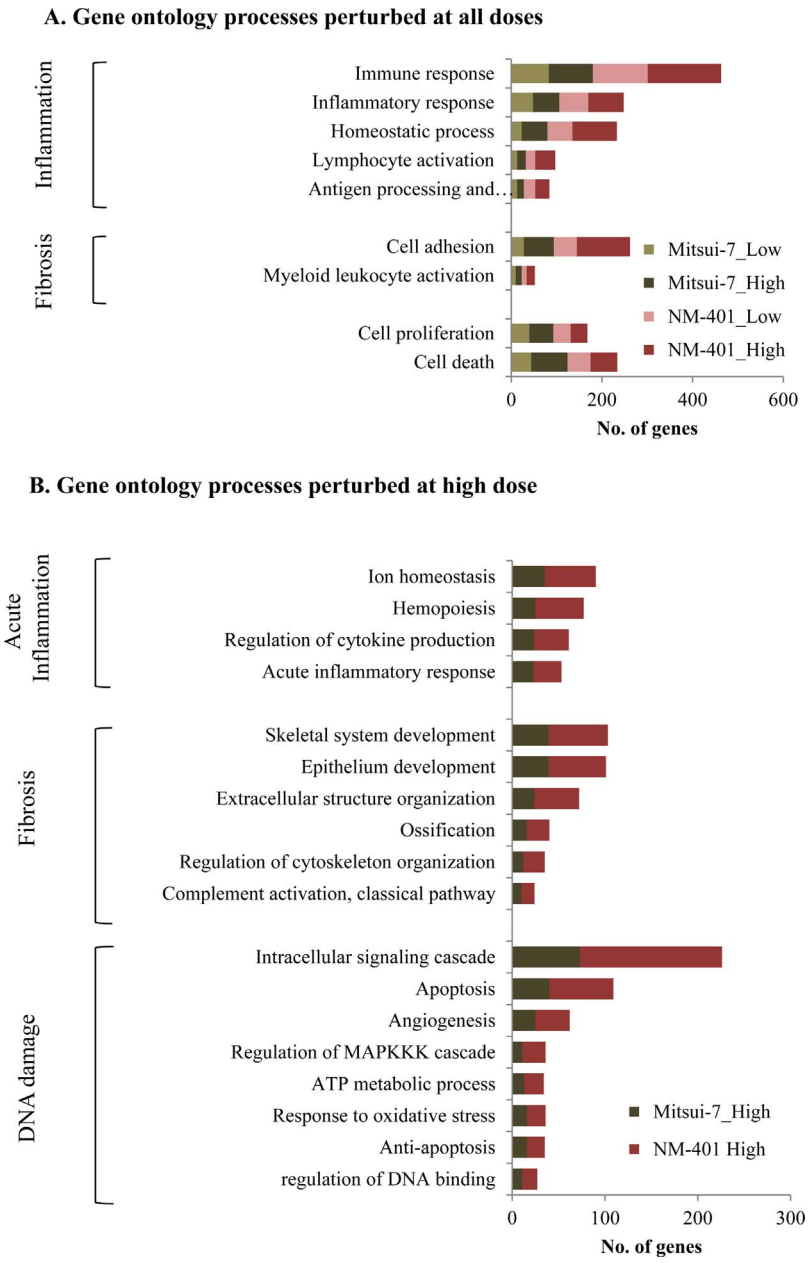

Fig. 9. Significant differentially perturbed biological pathways (p value ≤0.05) for Mitsui -7- or NM-401-treated lung tissues, which were common to all dose groups (A), and only perturbed in high dose groups (B) 90 days after the last exposure.

significant. Upstream regulators *Tnf*, interleukin 6 (*Il6*), *Myd88*, colony stimulating factors (*Csf1* and *Csf2*), interferon regulatory factor 7 (*Irf7*), Jun oncogene (*Jun*), insulin-like growth factor I (*Igf1*), nitric oxide synthase 2 (*Nos2*), *Cd44*, chemokine (C-C motif) ligand 2 (*Ccl2*), BCL2-associated X protein (*Bax*) and secreted phosphoprotein 1 (*Spp1*) were significantly activated (Supplementary Fig. 2C) in lung samples exposed to Mitsui-7 and NM-401 in both dose groups. The interleukin 10 receptor-alpha (*Il10ra*), atypical chemokine receptor 2, (*Ackr2*), suppressor of cytokine signaling 1 (*Socs1*) and apolipoprotein E precursor (*Apoe*) appeared to be inhibited (Z- score ≤2) in these groups. In addition, Mitsui-7 in the low and high dose groups and NM-401 in the high dose group inhibited regulation of prostaglandin E receptor 4 (Ptger4). However NM-401 inhibited regulation of interleukin 1 receptor antagonist (Il1rn).

A list of genes associated with inflammation and fibrosis was compiled using the Qiagen mouse RT^2 profiler Pathway-specific PCR array, and the MWCNT-induced gene list published in Poulsen et al., 2015 [6]. Similarly, we compiled a lung cancer gene list using the genes present on the Qiagen mouse RT^2 profiler array, and the MWCNT-induced 35 cancer gene signature reported in [67]. These lists were used to assess number of DEGs in lungs exposed to Mitsui -7 or NM-401 that are associated with inflammation, fibrosis and cancer (Fig. 10A–D). Following Mitsui -7 exposure, a total of 61 and 58 DEGs were associated with inflammation in the low and high dose groups, respectively (Fig. 10A and B), and 45 and 42 DEGs were associated with fibrosis in the low and high dose groups, respectively (Fig. 10A and B). Among the fibrotic genes, 37 genes in the low dose group (Fig. 10A) and 35 genes in the high dose group (Fig. 10B) were common to DEGs associated with inflammation. There were 27 DEGs in the low dose group (Fig. 10A) and 29 DEGs in the high dose group (Fig. 10B) that were associated with cancer, 8 of which were common to inflammation and fibrosis in each dose group (Fig. 10A–B).

For the NM-401 exposure, a total of 61 and 75 DEGs were associated with inflammation (Fig. 10C and D), and 42 and 55 DEGs were associated with fibrosis at the low and high doses, respectively (Fig. 10C and D). Among the fibrotic genes, 37 DEGs in the low dose group (Fig. 10C) and 42 DEGs in the high dose group (Fig. 10D) were also associated with inflammation. There were 29 DEGs in the low dose

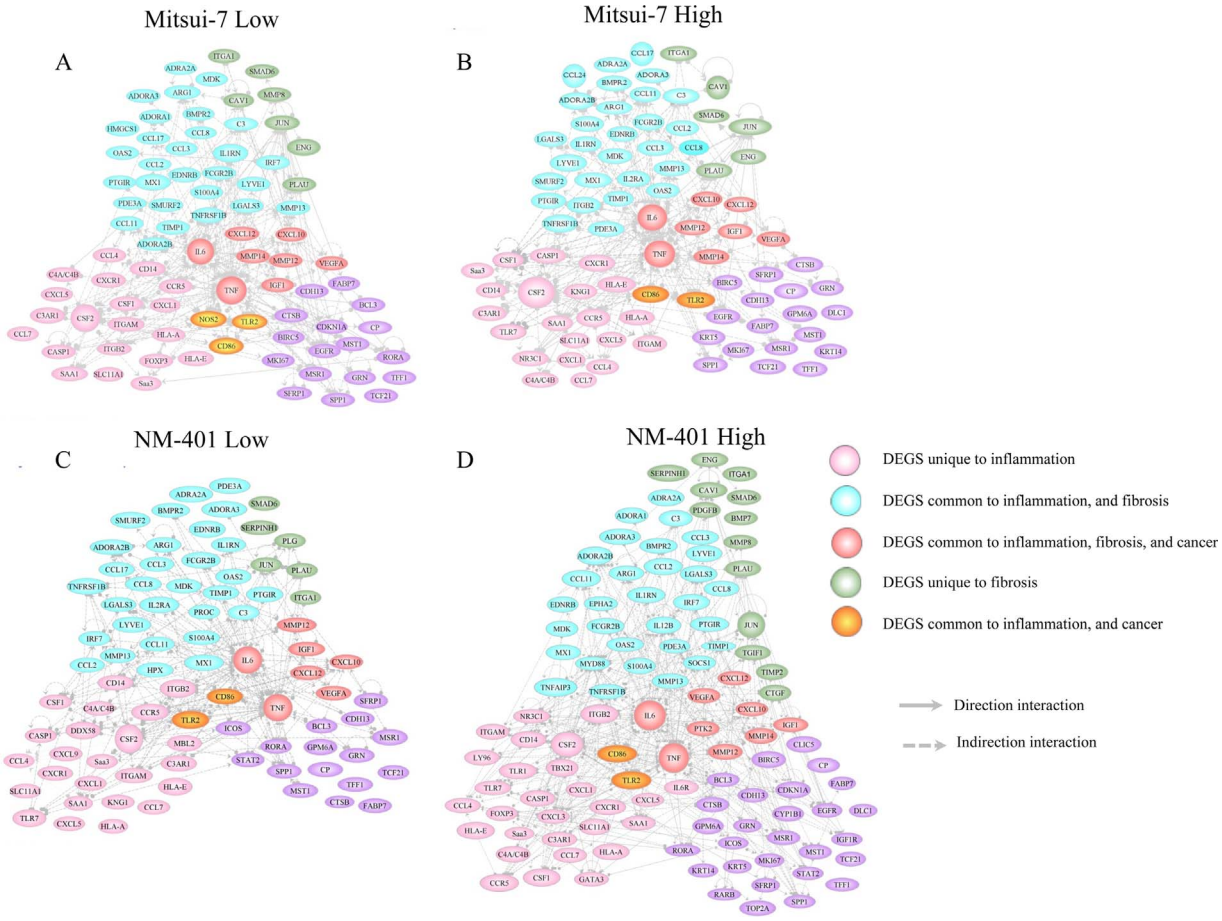

Fig. 10. Network showing direct and indirect interactions between significant differentially expressed genes (FDR p value ≤0.05) associated with lung inflammation, fibrosis and cancer. Expression changes observed in lung tissues from animals exposed to Mitsui -7 or NM-401, at low or high dose, 90 days after the last exposure.

group (Fig. 10C) and 39 DEGs in the high dose group (Fig. 10D) that were associated with cancer; 7 of these DEGs in the low dose group (Fig. 10C) and 9 in the high dose group (Fig. 10D) were common to inflammation and fibrosis. Approximately 20% of the fibrotic DEGs induced by Mitsui -7 or NM-401 (e.g., matrix metallopeptidase 12 (Mmp12), matrix metallopeptidase 14 (Mmp14), chemokine (C-X-C motif) ligand 10 (Cxcl10), insulin-like growth factor 1 (Igf1), interleukin 6 (Il6) and Ptk2) are also associated with cancer.

4. Discussion

In the present study, the transgenic Muta™Mouse system was used to investigate the ability of two rigid and straight MWCNT types (Mitsui-7 and NM-401) to induce *in vivo* DNA damage (i.e., strand breaks), transgene mutations, inflammation, cellular proliferation, p53 expression, global gene expression changes following multiple pulmonary exposures, in an attempt to elucidate the underlying mechanisms of potential carcinogenesis caused by these materials. Observations at 90 days post-exposure to four instillations of Mitsui-7, a type of MWCNT categorised by IARC as possibly carcinogenic to humans (2B), did not reveal any significant increase in DNA damage. No mutations were observed in the *lacZ* gene in lung tissue. In comparison, NM-401, another type of MWCNT, not classified as carcinogenic, induced significant DNA damage in mouse lungs in the 78 ± 5 μg/mouse dose group at the same time point; however, it did not induce mutations in the *lacZ* gene in lung tissue.

Depending on the type of MWCNTs, doses, and post-exposure time points investigated, the literature pertaining to induced DNA damage, such as strand breaks (i.e., comet results), is variable. The comet assay has been previously used to demonstrate that rigid and long MWCNTs can induce DNA strand breaks. For example, Poulsen et al. (2015) showed that NM-401 (straight and rigid fiber), but not NRCWE 026 (tangled fiber), induced DNA damage in lungs of animals collected 1 day after intratracheal exposure [6]. Similar results showing increased DNA strand breaks and adducts were observed in mice exposed to Mitsui-7 *via* intratracheal instillation [17], and DNA strand breaks in BALF of mice exposed to Mitsui-7 *via* inhalation [68]. Another study [69] showed significant DNA damage at human oxoguanine DNA glycosylase 1 (hOGG1)- and formamidopyrimidine DNA glycosylase (FPG)-sensitive sites (i.e., indicative of oxidative DNA lesions), but no significant increase in DNA damage in the lungs of *Apolipoprotein E*-deficient (*ApoE*−/−) mice following 10 intratracheal instillations of Mitsui-7 (i.e., 4 or 40 μg/mouse per week for 10 weeks). However NM-401 did not show DNA damage in A549, BEASE-2B and FE-1[33,70].

It has been shown that Mitsui-7 can increase *gpt* mutant frequencies in lungs of gpt delta transgenic mice 56 days after 4 repeated intratracheal instillation of 200 μg/mouse for four weeks [17]. On the other hand, single or double instillations did not induce a significant increase in *gpt* mutant frequencies. In addition, the *Pig-a* mutation assays in the bone marrow and the *gpt* delta mutation assays in lungs did not show an increase in mutations of F344/NSlc-Tg (*gpt*-delta) male rats administered a single intratracheal instillations of Mitsui-7 (1 mg/kg) [71]. I*n vitro,* exposures of Chinese hamster lung cells to Mitsui-7 also did not induce significant increases in hypoxanthine-guanine phosphoribosyltransferase (*hgprt*) mutations, micronuclei or chromosome aberrations [72]. Mutagenic effects of NM-401 have not very much been documented. In one study, *in vitro* exposure of Chinese hamster lung (V79) fibroblasts to NM-401 induced *hgprt* mutations [73]. One of

the limitations of the present study is that the post-exposure recovery period may be too short and may not be ideal to capture the mutations. A large fraction of the instilled CNT dose will remain in the lungs for more than a year [74], and it could be hypothesized that the observed pulmonary genotoxicity caused by NM-401 would develop into mutations following a longer post exposure period. However, at present, no international guidelines are available to investigate the genotoxic effects of MWCNTs, and the overall evidence regarding the mutagenicity of MWCNTs is scarce and inconsistent. These results suggest that more studies are needed to conclusively assess the *in vivo* genotoxic abilities of MWCNTs.

From the results, it can be construed that some types of MWCNTs have the potential to induce DNA strand breaks; however, several factors including the strain of mice investigated, dose regimen, mode of exposure and post-exposure time points for sampling employed may all have significant influence on the study conclusions. Although NM-401 induced DNA damage at the high dose tested, there was no evidence for gene mutations. It is a possibility that persistent MWCNTs (as observed by the microscopic analysis) leading to chronic tissue injury and cell death may have effectively removed the cells containing mutated genes before they were fixed leading to no changes in the overall mutant frequency in *lac*Z gene. The present study did not investigate chromosomal aberrations and micronuclei, other markers of genotoxicity and thus, the true implications of the observed DNA strand breaks on the lung remains unclear. However, there are studies in the literature that have investigated induction of chromosomal aberrations and micronuclei formation following exposure to MWCNTs. Authors [75] showed that industrial MWCNT graphistrength do not show any chromosomal damage or micronuclei formation in bone marrow of rats at 90 day post- exposure following nasal inhalation at dose of 5 mg/m^3. On the other hand, unmodified MWCNTs at a dose of 2–10 mg/kg body weight [76] and COOH functionalized MWCNT at a dose of 0.75 mg/kg body weight [16] were shown to induce chromosomal damage in bone marrow cells of Swiss Albino mice. NM-401 also induced chromosomal damage in A549 but not in BEAS-2B or in human lymphocytes [70,77]. COOH functionalized MWCNT were shown to induce dose dependent mitotic spindle damage in immortalized respiratory epithelial cells (BEAS-2B) at dose of 0.024–24 μg/cm^2 [78]; however, unmodified MWCNT did not induce any chromosomal damage in BEAS-2 B at a dose of 5–80 μg/cm^2 [79]. As mentioned above, it is also a possibility that MWCNTs are clastogens that induce disruption or breakage of chromosomes leading to rearrangement, large deletions or additions in chromosomes, a form of mutagenesis leading to genetic instability and cancer. However, this study has not investigated the clastogenic effects of MWCNTs. Thus, additional studies involving time series analysis and different genotoxic endpoints may help delineate the genotoxic effects of MWCNTs; moreover, elucidate the underlying mechanisms. It has been suggested that the underlying mechanisms of particle-induced genotoxity may not be the same as chemical-induced genotoxicity [75]. Genotoxicity may result from the direct interaction of substances with DNA, or from indirect effects including ROS synthesised by inflammatory cells during the substance-induced inflammation in lungs. Although there hasn't been evidence supporting the claim that MWCNTs are genotoxic carcinogens, it is clear from the studies described above that MWCNTs induce robust chronic lung inflammation involving multiple inflammatory cell types resulting in ROS generation and subsequent DNA damage. Although it can be argued that DNA damage may not be necessary for MWCNT-induced carcinogenesis, it can also be hypothesised that MWCNTs that induce both chronic inflammation and sustained DNA damage are more potent carcinogens (https://www.niehs.nih.gov/news/newsletter/2015/9/spotlight-mixtures/). Recently, IARC recognised 10 key characteristics of carcinogens, which included ability to induce chronic inflammation and tissue irritation [80], both of which are known to be the hallmark consequences of MWCNT exposure. The others include electrophilic nature, ability to induce genotoxicity, affect DNA repair mechanisms, induce oxidative stress, affect epigenetics, immunospressive, modulate receptor-mediated signalling, disrupts cell cycle, and cell proliferation [80].

Non-genotoxic carcinogens include substances that act as tumor promoters, endocrine disruptors, receptor mediators, immune suppressors, or inflammogenic and tissue damaging agents [81] and may act *via* disruption of cellular structures and vesicles (lysosomal degradation), increased cellular proliferation or by modulating the processes involved in DNA repair or in the maintenance of genetic stability. Here, we show that MWCNTs persist in lungs long after the exposure is terminated. Moreover, our results show that chronic lung inflammation and markers of lung fibrosis are found 90 days post-exposure. These can in turn cause increased ROS synthesis and chronic tissue injury that may be predisposing factors for carcinogenesis. Furthermore, the gene expression analysis was extended to identify focus molecules or DEGs that are highly connected to the biological processes and/or disease related networks available in the IPA database. Our results showed that cancer was the top ranking IPA network perturbed with 31 focus molecules in lung tissues exposed to Mitsui-7 at the lowest dose. Cancer, cell death and survival, and ROS generation were among the top networks, ranked 4th, 3rd, and 16th, respectively, perturbed in lung tissues exposed to high dose Mitsui-7 with 28, 29, and 24 focus molecules, respectively. Cancer, cell death and survival, and ROS generation were also among the top 25 networks, ranked 23rd, 25th, and 21st, respectively, perturbed in lung tissues exposed to low dose NM-401 with 21, 20, and 21 focus molecules, respectively. Cancer was the 12th ranked network with 31 focus molecules in lung tissues exposed to NM-401 at high dose. Regardless of the genetic toxicity results, the results clearly indicate that the two types of MWCNTs examined induced a significant enrichment of genes involved in cancer pathways and networks.

A detailed analysis of the tissue-wide gene expression changes showed that genes associated with scavenging free radicals such as, BCL2-like 14 (apoptosis facilitator,*Bcl2l14*), betaine-homocysteine methyltransferase 2 (*Bhmt*), cytochrome b-245, beta polypeptide (*Cybb*), Epstein-Barr virus induced gene 3 (*Ebi3*), c-fos induced growth factor (*Figf*), insulin-like growth factor binding proteins (*Igfbp1*, *Igfbp6*), insulin-like 6 (*Insl6*), neutrophil cytosolic factors (*Ncf1*,*Ncf2*,*Ncf4*), NADPH oxidase 4 (*Nox4*), NADPH oxidase organizer 1 (*Noxo1*), oncostatin M receptor (*Osmr*), platelet-derived growth factor, C polypeptide (*Pdgfc*), prominin 1 (*Prom1*), trefoil factor 2 (spasmolytic protein 1) (*Tff2*), transmembrane protein with EGF-like and two follistatin-like domains 2 (*Tmeff2*) were significantly differentially expressed in lungs of animals exposed to the high dose of Mitsui-7 and both doses of NM-401, suggesting perturbation of the redox status following exposure to MWCNTs. The significant alteration in ROS counteracting genes is supportive of the observed DNA strand break results for NM-401 groups. Although, ROS can cause DNA strand breaks and mutations [60,82,83], repairs of the DNA lesions and breaks by repair enzymes at an early stage can prevent associated mutagenic activity [84]. As described above, it is also possible that cells with damaged DNA are committed to apoptosis, hence DNA damage was not observed in Mitsui-7 groups in spite of significant alteration of ROS counteracting genes. Indeed, expression of several genes that are involved in cell death were altered by both MWCNT types including: (a) upregulation of mucosa associated lymphoid tissue lymphoma translocation gene 1 (*Malt1*), caspase 1 (*Casp 1*), caspase 4 (*Casp 4*), NIMA Related Kinase 6 (*Nek6*), cell death-inducing DFFA-like effector b (*Cideb*), programmed cell death 1 (*Pdcd1*), B-cell leukemia/lymphoma 2 related protein A1c (*Bcl2a1*), PYD and CARD domain (*Pycard*), baculoviral IAP repeat-containing (*Birc*), growth arrest and DNA-damage-inducible 45 gamma (*Gadd45 g*), NLR family, apoptosis inhibitory protein 2 (*Naip2*), and clusterin (*Clu*); and (b) downregulation of GATA zinc finger domain containing 2A (*Gatad2a*), cell death effector c (*Cidec*), tumor necrosis factor receptor superfamily, member 1b (*Tnfrsf1b*), Fas apoptotic inhibitory molecule 2 (*Fame2*) and endothelin converting enzyme 1 (*Ece 1*). Moreover, high levels of p53 expression were observed in the

fibrotic lesions of lungs in mice exposed to NM-401 showing significant increases in DNA strand break levels. p53 expression may be upregulated as a response to DNA damage caused by apoptosis. Our gene expression analysis showed significant differential expression of proapoptotic *Noxa1* and *Bax,* which can be induced in a p53 mediated apoptotic pathway [85]. Increased p53 expression in the fibrotic regions suggests the vulnerability of the disease foci for genetic damage and possible carcinogenic transformation if defence mechanisms such as p53 activation fail. Activation of p53 pathway is suggested to have a role in contributing tissue damage [86]. Increased p53 expression and fibrotic lesions were also observed in Mitsui-7 exposed lung despite clear evidence of DNA damage; however p53 expression was much lower in Mitsui-7 exposed lungs compared to NM-401 exposed lungs.

Genes from the mucin family were also altered following exposure to both types of MWCNTs. Membrane associated mucins, and both secreted gel forming and non-gel forming mucins, are involved in forming physical barriers, protecting and repairing epithelia against environmental toxins [87]. Elevated expression of membrane associated mucin, *Muc4*, secreted gel forming mucins *Muc5b* and *Muc5ac* occurred following exposure to selected doses of Mitsui-7 and NM-401 (i.e., high and low). However, *Muc1* was downregulated in all the experimental groups. Muc4 is thought to promote tumorigenesis through its epidermal growth factor (EGF)-like domain [88,89]. Increased expression of *Muc5b* is observed in the early stages of mucinous lung adenocarcinoma [90–92]. Upregulation of *Muc4*, *Muc5b* and *Muc5ac* and downregulation of *Muc1* is correlated with p53 mediated suppression of growth arrest by promoting apoptotic target [91]. In our study, histopathological analysis showed airway epithelial mucous metaplasia in lungs exposed to Mitsui-7 or NM-401 at all doses. These results suggest that even if the two MWCNT types were capable of inducing DNA damage, strong counteracting responses mounted against the generated ROS, and efficient and timely elimination of damaged cells through cell death, may have prevented accumulation of DNA damage and hence mutations at the post-exposure time point investigated. However, parallel increases or decreases in the expression of genes involved in cell survival, cell proliferation, anti-apoptotic processes, angiogenesis, combined with perturbations of the associated functions/pathways in tissues containing persistent fibres that manifest chronic inflammation and tissue irritation, may all enable creation of carcinogenic environment and ultimately carcinogenesis.

5. Conclusions

This study showed that repeated instillations of high doses of Mitsui-7 and NM-401, representing straight rigid carbon nanofibers, do not induce DNA mutations in transgenic MutaMouse at 90-days post-exposure. DNA strand breaks were only observed in lungs of animals exposed to NM-401, and not Mitsui-7. The observed DNA strand breaks in NM-401 were accompanied by increased p53 expression, which was specifically localised to fibrotic lesions, implying potential vulnerability of the fibrotic tissue to DNA damage. Neither DNA damage, nor p53 activation was observed in Mitsui-7 exposed mouse lungs to the same extent as that observed in the NM-401 group. However, both MWCNTs induced robust and chronic inflammation and fibrotic lesions in lungs. More importantly, both MWCNTs induced changes in the expression of hundreds of genes associated with hallmarks of cancer – cellular process involved in maintenance of cell homeostasis as well as activation of carcinogenic transformation. The results also indicated that a subset of DEGs associated with inflammation and fibrosis are also linked to cancer. More studies involving chronic exposures to low doses of MWCNTs, with investigations of induced alterations in cellular activities related to DNA repair, activation of cellular death cascades, and other neoplastic transformation processes are necessary to fully appreciate the carcinogenic potential of toxic fibres such as MWCNTs.

Acknowledgements

This work was supported by Health Canada's Genomics Research and Development Initiative and Chemicals Management Plan2-nano, the Danish Council of Independent Research (Medical Sciences, grant No. 6110-00103), and the Danish Centre for Nanosafety II.

We thank Ms. Christine Lemieux and Dr. Nikolai Chepelev for the helpful comments on the manuscript. We also thank Lynda Soper and John Gingrich for conducting *lac*Z mutant frequency analysis.

Appendix A. Supplementary data

Supplementary data associated with this article can be found, in the online version, at http://dx.doi.org/10.1016/j.mrgentox.2017.08.005.

References

[1] K.A. Jensen, J. Bøgelund, P. Jackson, N.R. Jacobsen, R. Birkedal, P.A. Clausen, A.T. Saber, H. Wallin, U. Vogel, Carbon Nanotubes – Types, Products, Market, and Provisional Assessment of the Associated Risks to Man and the Environment, Environmental Project No. 1805. 1–150, The Danish Environmental Protection Agency, DK-1401 Copenhagen K, 2015.
[2] B. Czarny, D. Georgin, F. Berthon, G. Plastow, M. Pinault, G. Patriarche, A. Thuleau, M.M. L'Hermite, F. Taran, V. Dive, Carbon nanotube translocation to distant organs after pulmonary exposure: insights from in situ (14)C-radiolabeling and tissue radioimaging, ACS Nano 8 (2014) 5715–5724.
[3] N.R. Jacobsen, P. Møller, P.A. Clausen, A.T. Saber, C. Micheletti, K.A. Jensen, H. Wallin, U. Vogel, Biodistribution of carbon nanotubes in animal models, Basic Clin. Pharmacol. Toxicol. (2016) 1–14.
[4] C. Kobler, S.S. Poulsen, A.T. Saber, N.R. Jacobsen, H. Wallin, C.L. Yauk, S. Halappanavar, U. Vogel, K. Qvortrup, K. Molhave, Time-dependent subcellular distribution and effects of carbon nanotubes in lungs of mice, PLoS One 10 (2015) 1–17.
[5] S. Poulsen, N.R. Jacobsen, S. Labib, D. Wu, M. Husain, A. Williams, J.P. Bøgelund, O. Andersen, C. Køble, K. Mølhave, Z.O. Kyjovska, A.T. Saber, H. Wallin, C.L. Yauk, U. Vogel, S. Halappanavar, Transcriptomic analysis reveals novel mechanistic insight into murine biological responses to multi-walled carbon nanotubes in lungs and cultured lung epithelial cells, PLoS One 8 (2013) e80452.
[6] S.S. Poulsen, A.T. Saber, A. Williams, O. Andersen, C. Kobler, R. Atluri, M.E. Pozzebon, S.P. Mucelli, M. Simion, D. Rickerby, A. Mortensen, P. Jackson, Z.O. Kyjovska, K. Molhave, N.R. Jacobsen, K.A. Jensen, C.L. Yauk, H. Wallin, S. Halappanavar, U. Vogel, MWCNTs of different physicochemical properties cause similar inflammatory responses, but differences in transcriptional and histological markers of fibrosis in mouse lungs, Toxicol. Appl. Pharmacol. 284 (2015) 16–32.
[7] S.S. Poulsen, P. Jackson, K. Kling, K.B. Knudsen, V. Skaug, Z.O. Kyjovska, B.L. Thomsen, P.A. Clausen, R. Atluri, T. Berthing, S. Bengtson, H. Wolff, K.A. Jensen, H. Wallin, U. Vogel, Multi-walled carbon nanotube physicochemical properties predict pulmonary inflammation and genotoxicity, Nanotoxicology 10 (2016) 1263–1275.
[8] R.R. Mercer, J.F. Scabilloni, A.F. Hubbs, L. Wang, L.A. Battelli, W. McKinney, V. Castranova, D.W. Porter, Extrapulmonary transport of MWCNT following inhalation exposure, Part. Fibre Toxicol. 10 (2013) 1–13.
[9] D.W. Porter, A.F. Hubbs, R.R. Mercer, N. Wu, M.G. Wolfarth, K. Sriram, S. Leonard, L. Battelli, D. Schwegler-Berry, S. Friend, Mouse pulmonary dose- and time course-responses induced by exposure to multi-walled carbon nanotubes, Toxicology 269 (2010) 136–147.
[10] D.W. Porter, A.F. Hubbs, B.T. Chen, W. McKinney, R.R. Mercer, M.G. Wolfarth, L. Battelli, N. Wu, K. Sriram, S. Leonard, M. Andrew, P. Willard, S. Tsuruoka, M. Endo, T. Tsukada, F. Munekane, D.G. Frazer, V. Castranova, Acute pulmonary dose-responses to inhaled multi-walled carbon nanotubes, Nanotoxicology 7 (2012) 1179–1194.
[11] T.A. Wynn, Integrating mechanisms of pulmonary fibrosis, J. Exp. Med. 208 (2011) 1339–1350.
[12] S. Rittinghausen, A. Hackbarth, O. Creutzenberg, H. Ernst, U. Heinrich, A. Leonhardt, D. Schaudien, The carcinogenic effect of various multi-walled carbon nanotubes (MWCNTs) after intraperitoneal injection in rats, Part. Fibre Toxicol. 11 (2014) 1–18.
[13] Y. Sakamoto, D. Nakae, N. Fukumori, K. Tayama, A. Maekawa, K. Imai, A. Hirose, T. Nishimura, N. Ohashi, A. Ogata, Induction of mesothelioma by a single intrascrotal administration of multi-wall carbon nanotube in intact male Fischer 344 rats, J. Toxicol. Sci. 34 (2009) 65–76.
[14] A. Takagi, A. Hirose, T. Nishimura, N. Fukumori, A. Ogata, N. Ohashi, S. Kitajima, J. Kanno, Induction of mesothelioma in p53+/− mouse by intraperitoneal application of multi-wall carbon nanotube, J. Toxicol. Sci. 33 (2008) 105–116.
[15] A. Takagi, A. Hirose, M. Futakuchi, H. Tsuda, J. Kanno, Dose-dependent mesothelioma induction by intraperitoneal administration of multi-wall carbon nanotubes in p53 heterozygous mice, Cancer Sci. 103 (2012) 1440–1444.
[16] A.K. Patlolla, S.M. Hussain, J.J. Schlager, S. Patlolla, P.B. Tchounwou, Comparative study of the clastogenicity of functionalized and nonfunctionalized multiwalled carbon nanotubes in bone marrow cells of Swiss-Webster mice, Environ. Toxicol. 25

(2010) 608–621.
[17] T. Kato, Y. Totsuka, K. Ishino, Y. Matsumoto, Y. Tada, D. Nakae, S. Goto, S. Masuda, S. Ogo, M. Kawanishi, T. Yagi, T. Matsuda, M. Watanabe, K. Wakabayashi, Genotoxicity of multi-walled carbon nanotubes in both in vitro and in vivo assay systems, Nanotoxicology 7 (2013) 452–461.
[18] K. Aschberger, H.J. Johnston, V. Stone, R.J. Aitken, S.M. Hankin, S.A. Peters, C.L. Tran, F.M. Christensen, Review of carbon nanotubes toxicity and exposure-appraisal of human health risk assessment based on open literature, Crit. Rev. Toxicol. 40 (2010) 759–790.
[19] Y. Grosse, D. Loomis, K.Z. Guyton, B. Lauby-Secretan, G.F. El, V. Bouvard, L. Benbrahim-Tallaa, N. Guha, C. Scoccianti, H. Mattock, K. Straif, Carcinogenicity of fluoro-edenite, silicon carbide fibres and whiskers, and carbon nanotubes, Lancet Oncol. 15 (2014) 1427–1428.
[20] T. Kasai, Y. Umeda, M. Ohnishi, T. Mine, H. Kondo, T. Takeuchi, M. Matsumoto, S. Fukushima, Lung carcinogenicity of inhaled multi-walled carbon nanotube in rats, Part. Fibre Toxicol. 13 (2016) 1–19.
[21] C.A. Poland, R. Duffin, I. Kinloch, A. Maynard, W.A.H. Wallace, A. Seaton, V. Stone, S. Brown, W. MacNee, K. Donaldson, Carbon nanotubes introduced into the abdominal cavity of mice show asbestos-like pathogenicity in a pilot study, Nat. Nano 3 (2008) 423–428.
[22] H. Nagai, Y. Okazaki, S.H. Chew, N. Misawa, Y. Yamashita, S. Akatsuka, T. Ishihara, K. Yamashita, Y. Yoshikawa, H. Yasui, L. Jiang, H. Ohara, T. Takahashi, G. Ichihara, K. Kostarelos, Y. Miyata, H. Shinohara, S. Toyokuni, Diameter and rigidity of multiwalled carbon nanotubes are critical factors in mesothelial injury and carcinogenesis, Proc. Natl. Acad. Sci. U. S. A. 108 (2011) E1331–E1338.
[23] H. Nagai, Y. Okazaki, S.H. Chew, N. Misawa, Y. Miyata, H. Shinohara, S. Toyokuni, Intraperitoneal administration of tangled multiwalled carbon nanotubes of 15 nm in diameter does not induce mesothelial carcinogenesis in rats, Pathol. Int. 63 (2013) 457–462.
[24] R.K. Srivastava, A.B. Pant, M.P. Kashyap, V. Kumar, M. Lohani, L. Jonas, Q. Rahman, Multi-walled carbon nanotubes induce oxidative stress and apoptosis in human lung cancer cell line-A549, Nanotoxicology 5 (2011) 195–207.
[25] H. Patel, S. Kwon, Multi-walled carbon nanotube-induced inflammatory response and oxidative stress in a dynamic cell growth environment, J. Biol. Eng. 6 (2012) 22.
[26] D.M. Brown, K. Donaldson, V. Stone, Nuclear translocation of Nrf2 and expression of antioxidant defence genes in THP-1 cells exposed to carbon nanotubes, J. Biomed. Nanotechnol. 6 (2010) 224–233.
[27] A.K. Patlolla, A. Berry, P.B. Tchounwou, Study of hepatotoxicity and oxidative stress in male Swiss-Webster mice exposed to functionalized multi-walled carbon nanotubes, Mol. Cell. Biochem. 358 (2011) 189–199.
[28] L.M. Sargent, D.W. Porter, L.M. Staska, A.F. Hubbs, D.T. Lowry, L. Battelli, K.J. Siegrist, M.L. Kashon, R.R. Mercer, A.K. Bauer, B.T. Chen, J.L. Salisbury, D. Frazer, W. McKinney, M. Andrew, S. Tsuruoka, M. Endo, K.L. Fluharty, V. Castranova, S.H. Reynolds, Promotion of lung adenocarcinoma following inhalation exposure to multi-walled carbon nanotubes, Part. Fibre Toxicol. 11 (2014) 1–18.
[29] P.A. Jeggo, L.H. Pearl, A.M. Carr, DNA repair, genome stability and cancer: a historical perspective, Nat. Rev. Cancer 16 (2016) 35–42.
[30] O. Auerbach, L. Garfinkel, V.R. Parks, Scar cancer of the lung: increase over a 21 year period, Cancer 43 (1979) 636–642.
[31] A.C. MacKinnon, J. Kopatz, T. Sethi, The molecular and cellular biology of lung cancer: identifying novel therapeutic strategies, Br. Med. Bull. 95 (2010) 47–61.
[32] Y.Y. Yu, P.F. Pinsky, N.E. Caporaso, N. Chatterjee, M. Baumgarten, P. Langenberg, J.P. Furuno, Q. Lan, E.A. Engels, Lung cancer risk following detection of pulmonary scarring by chest radiography in the prostate, lung, colorectal, and ovarian cancer screening trial, Arch. Intern. Med. 168 (2008) 2326–2332.
[33] P. Jackson, K. Kling, K.A. Jensen, P.A. Clausen, A.M. Madsen, H. Wallin, U. Vogel, Characterization of genotoxic response to 15 multiwalled carbon nanotubes with variable physicochemical properties including surface functionalizations in the FE1-Muta(TM) mouse lung epithelial cell line, Environ. Mol. Mutagen. 56 (2015) 183–203.
[34] The Nanogentox group, Facilitating the Safety Evaluation of Manufactured Nanomaterials By Characterising Their Potential Genotoxicity Hazard, (2013).
[35] N.R. Jacobsen, T. Stoeger, S. van den Brule, A.T. Saber, A. Beyerle, G. Vietti, A. Mortensen, J. Szarek, H.C. Budtz, A. Kermanizadeh, A. Banerjee, N. Ercal, U. Vogel, H. Wallin, P. Møller, Acute and subacute pulmonary toxicity and mortality in mice after intratracheal instillation of ZnO nanoparticles in three laboratories, Food Chem. Toxicol. 85 (2015) 84–95.
[36] M. Husain, D. Wu, A.T. Saber, N. Decan, N.R. Jacobsen, A. Williams, C.L. Yauk, H. Wallin, U. Vogel, S. Halappanavar, Intratracheally instilled titanium dioxide nanoparticles translocate to heart and liver and activate complement cascade in the heart of C57BL/6 mice, Nanotoxicology 9 (2015) 1013–1022.
[37] B.N. Snyder-Talkington, J. Dymacek, D.W. Porter, M.G. Wolfarth, R.R. Mercer, M. Pacurari, J. Denvir, V. Castranova, Y. Qian, N.L. Guo, System-based identification of toxicity pathways associated with multi-walled carbon nanotube-induced pathological responses, Toxicol. Appl. Pharmacol. 272 (2013) 476–489.
[38] E.J. Park, W.S. Cho, J. Jeong, J. Yi, K. Choi, K. Park, Pro-inflammatory and potential allergic responses resulting from B cell activation in mice treated with multi-walled carbon nanotubes by intratracheal instillation, Toxicology 259 (2009) 113–121.
[39] A.A. Shvedova, E. Kisin, A.R. Murray, V.J. Johnson, O. Gorelik, S. Arepalli, A.F. Hubbs, R.R. Mercer, P. Keohavong, N. Sussman, Inhalation vs. aspiration of single-walled carbon nanotubes in C57BL/6 mice: inflammation, fibrosis, oxidative stress, and mutagenesis, Am. J. Physiol. Lung Cell. Mol. Physiol. 295 (2008) L552–L565.
[40] National Institute for Occupational Safety and Health (NIOSH), Current Intelligence Bulletin 65: Occupational Exposure to Carbon Nanotubes and Nanofibers, U.S. Department of Health and Human Service. Centers for Disease Control and Prevention. Publication No. 2013–145, 2013.
[41] L. Ma-Hock, S. Treumann, V. Strauss, S. Brill, F. Luizi, M. Mertler, K. Wiench, A.O. Gamer, B. van Ravenzwaay, R. Landsiedel, Inhalation toxicity of multiwall carbon nanotubes in rats exposed for 3 months, Toxicol. Sci. 112 (2009) 468–481.
[42] J.H. Lee, S.B. Lee, G.N. Bae, K.S. Jeon, J.U. Yoon, J.H. Ji, J.H. Sung, B.G. Lee, J.H. Lee, J.S. Yang, H.Y. Kim, C.S. Kang, I.J. Yu, Exposure assessment of carbon nanotube manufacturing workplaces, Inhal. Toxicol. 22 (2010) 369–381.
[43] J.H. Han, E.J. Lee, J.H. Lee, K.P. So, Y.H. Lee, G.N. Bae, S.B. Lee, J.H. Ji, M.H. Cho, I.J. Yu, Monitoring multiwalled carbon nanotube exposure in carbon nanotube research facility, Inhal. Toxicol. 20 (2008) 741–749.
[44] M. Methner, C. Beaucham, C. Crawford, L. Hodson, C. Geraci, Field application of the Nanoparticle Emission Assessment Technique (NEAT): task-based air monitoring during the processing of engineered nanomaterials (ENM) at four facilities, J. Occup. Environ. Hyg. 9 (2012) 543–555.
[45] M. Hedmer, L. Ludvigsson, C. Isaxon, P.T. Nilsson, V. Skaug, M. Bohgard, J.H. Pagels, M.E. Messing, H. Tinnerberg, Detection of multi-walled carbon nanotubes and carbon nanodiscs on workplace surfaces at a small-scale producer, Ann. Occup. Hyg. 59 (2015) 836–852.
[46] M.E. Birch, B.K. Ku, D.E. Evans, T.A. Ruda-Eberenz, Exposure and emissions monitoring during carbon nanofiber production—part I: elemental carbon and iron-soot aerosols, Ann. Occup. Hyg. 55 (2011) 1016–1036.
[47] M.E. Birch, Exposure and emissions monitoring during carbon nanofiber production-part II: polycyclic aromatic hydrocarbons, Ann. Occup. Hyg. 55 (2011) 1037–1047.
[48] L. Mikkelsen, M. Sheykhzade, K.A. Jensen, A.T. Saber, N.R. Jacobsen, U. Vogel, H. Wallin, S. Loft, P. Moller, Modest effect on plaque progression and vasodilatory function in atherosclerosis-prone mice exposed to nanosized TiO(2), Part Fibre Toxicol. 8 (2011) 32.
[49] P.S. Shwed, J. Crosthwait, G.R. Douglas, V.L. Seligy, Characterisation of MutaMouse lambdagt10-lacZ transgene: evidence for in vivo rearrangements, Mutagenesis 25 (2010) 609–616.
[50] J.A. Gossen, W.J. de Leeuw, C.H. Tan, E.C. Zwarthoff, F. Berends, P.H. Lohman, D.L. Knook, J. Vijg, Efficient rescue of integrated shuttle vectors from transgenic mice: a model for studying mutations in vivo, Proc. Natl. Acad. Sci. U. S. A. 86 (1989) 7971–7975.
[51] S. Labib, C. Yauk, A. Williams, V.M. Arlt, D.H. Phillips, P.A. White, S. Halappanavar, Subchronic oral exposure to benzo(a)pyrene leads to distinct transcriptomic changes in the lungs that are related to carcinogenesis, Toxicol. Sci. 129 (2012) 213–224.
[52] I.B. Lambert, T.M. Singer, S.E. Boucher, G.R. Douglas, Detailed review of transgenic rodent mutation assays, Mutat. Res. 590 (2005) 1–280.
[53] R. Renne, A. Brix, J. Harkema, R. Herbert, B. Kittel, D. Lewis, Proliferative and nonproliferative lesions of the rat and mouse respiratory tract, Toxicol. Pathol. 37 (2009) 1533–1601.
[54] S. Aziz, S. Pervez, S. Khan, T. Siddiqui, N. Kayani, M. Israr, M. Rahbar, Case control study of novel prognostic markers and disease outcome in pregnancy/lactation-associated breast carcinoma, Pathol. Res. Pract. 199 (2003) 15–21.
[55] F. Kurshumliu, L. Gashi-Luci, S. Kadare, M. Alimehmeti, U. Gozalan, Classification of patients with breast cancer according to Nottingham prognostic index highlights significant differences in immunohistochemical marker expression, World J. Surg. Oncol. 12 (2014) 1–5.
[56] S.Y. Yoon, G.H. Hong, H.S. Kwon, S. Park, S.Y. Park, B. Shin, T.B. Kim, H.B. Moon, Y.S. Cho, S-adenosylmethionine reduces airway inflammation and fibrosis in a murine model of chronic severe asthma via suppression of oxidative stress, Exp. Mol. Med. 48 (2016) e236.
[57] D.K. Fritz, C. Kerr, R. Fattouh, A. Llop-Guevara, W.I. Khan, M. Jordana, C.D. Richards, A mouse model of airway disease: oncostatin M-induced pulmonary eosinophilia, goblet cell hyperplasia, and airway hyperresponsiveness are STAT6 dependent, and interstitial pulmonary fibrosis is STAT6 independent, J. Immunol. 186 (2011) 1107–1118.
[58] P. Jackson, L.M. Pedersen, Z.O. Kyjovska, N.R. Jacobsen, A.T. Saber, K.S. Hougaard, U. Vogel, H. Wallin, Validation of freezing tissues and cells for analysis of DNA strand break levels by comet assay, Mutagenesis 28 (2013) 699–707.
[59] T. Chen, J. Yan, Y. Li, Genotoxicity of titanium dioxide nanoparticles, J. Food Drug Anal. 22 (2014) 95–104.
[60] N.R. Jacobsen, A.T. Saber, P. White, P. Moller, G. Pojana, U. Vogel, S. Loft, J. Gingerich, L. Soper, G.R. Douglas, H. Wallin, Increased mutant frequency by carbon black, but not quartz, in the lacZ and cII transgenes of muta mouse lung epithelial cells, Environ. Mol. Mutagen. 48 (2007) 451–461.
[61] S. Halappanavar, J. Nikota, D. Wu, A. Williams, C.L. Yauk, M. Stampfli, IL-1 receptor regulates microRNA-135b expression in a negative feedback mechanism during cigarette smoke-induced inflammation, J. Immunol. Author Choice 190 (2013) 3679–3686.
[62] H. Wu, M.K. Kerr, X. Cui, G. Churchill, MAANOVA. A software package for the analysis of spotted cDNA microarray experiments, in: G. Parmigiani, E. Garrett, R. Irizarry, S. Zeger (Eds.), The Analysis of Gene Expression Data, Springer, New York, 2003, pp. pp. 313–341.
[63] X. Cui, J.T. Hwang, J. Qiu, N.J. Blades, G.A. Churchill, Improved statistical tests for differential gene expression by shrinking variance components estimates 1, Biostatistics 6 (2005) 59–75.
[64] Y. Benjamini, Y. Hochberg, Controlling the false discovery rate: a practical and powerful approach to multiple testing, J. R. Stat. Soc. Ser. B (Methodol.) 57 (1995) 289–300.
[65] D.W. Huang, B.T. Sherman, R.A. Lempicki, Bioinformatics enrichment tools: paths

toward the comprehensive functional analysis of large gene lists, Nucleic Acids Res. 37 (2009) 1–13.
[66] C.A. Austin, G.K. Hinkley, A.R. Mishra, Q. Zhang, T.H. Umbreit, M.W. Betz, E. Wildt, B.J. Casey, S. Francke-Carroll, S.M. Hussain, S.M. Roberts, K.M. Brown, P.L. Goering, Distribution and accumulation of 10 nm silver nanoparticles in maternal tissues and visceral yolk sac of pregnant mice, and a potential effect on embryo growth, Nanotoxicology 10 (2016) 654–661.
[67] N.L. Guo, Y.W. Wan, J. Denvir, D.W. Porter, M. Pacurari, M.G. Wolfarth, V. Castranova, Y. Qian, Multi-walled carbon nanotube-induced gene signatures in the mouse lung: potential predictive value for human lung cancer risk and prognosis, J. Toxicol. Environ. Health A 75 (2012) 1129–1153.
[68] J. Catalán, K.M. Siivola, P. Nymark, H. Lindberg, S. Suhonen, H. Järventaus, A.J. Koivisto, C. Moreno, E. Vanhala, H. Wolff, K.I. Kling, K.A. Jensen, K. Savolainen, H. Norppa, In vitro and in vivo genotoxic effects of straight versus tangled multi-walled carbon nanotubes, Nanotoxicology 10 (2016) 794–806.
[69] D.V. Christophersen, N.R. Jacobsen, M.H. Andersen, S.P. Connell, K.K. Barfod, M.B. Thomsen, M.R. Miller, R. Duffin, J. Lykkesfeldt, U. Vogel, H. Wallin, S. Loft, M. Roursgaard, P. Moller, Cardiovascular health effects of oral and pulmonary exposure to multi-walled carbon nanotubes in ApoE-deficient mice, Toxicology 371 (2016) 29–40.
[70] H. Louro, M. Pinhão, J. Santos, A. Tavares, N. Vital, M. João Silva, Evaluation of the cytotoxic and genotoxic effects of benchmark multi-walled carbon nanotubes in relation to their physicochemical properties, Toxicol. Lett. 262 (2016) 123–134.
[71] K. Horibata, A. Ukai, A. Ogata, D. Nakae, H. Ando, Y. Kubo, A. Nagasawa, K. Yuzawa, M. Honma, Absence of in vivo mutagenicity of multi-walled carbon nanotubes in single intratracheal instillation study using F344 gpt delta rats, Genes Environ. 39 (2017) 1–5.
[72] M. Asakura, T. Sasaki, T. Sugiyama, M. Takaya, S. Koda, K. Nagano, H. Arito, S. Fukushima, Genotoxicity and cytotoxicity of multi-wall carbon nanotubes in cultured Chinese hamster lung cells in comparison with chrysotile A fibers, J. Occup. Health 52 (2010) 155–166.
[73] L. Rubio, Y.N. El, A. Kazimirova, M. Dusinska, R. Marcos, Multi-walled carbon nanotubes (NM401) induce ROS-mediated HPRT mutations in Chinese hamster lung fibroblasts, Environ. Res. 146 (2016) 185–190.
[74] N.R. Jacobsen, P. Møller, P.A. Clausen, A.T. Saber, C. Micheletti, K.A. Jensen, H. Wallin, U. Vogel, Biodistribution of carbon nanotubes in animal models, Basic Clin. Pharmacol. Toxicol. (2017) 1–14.
[75] D. Pothmann, S. Simar, D. Schuler, E. Dony, S. Gaering, J.L. Le Net, Y. Okazaki, J.M. Chabagno, C. Bessibes, J. Beausoleil, F. Nesslany, J.F. Regnier, Lung inflammation and lack of genotoxicity in the comet and micronucleus assays of industrial multiwalled carbon nanotubes Graphistrength((c)) C100 after a 90-day nose-only inhalation exposure of rats, Part. Fibre Toxicol. 12 (2015) 4–28.
[76] M. Ghosh, A. Chakraborty, M. Bandyopadhyay, A. Mukherjee, Multi-walled carbon nanotubes (MWCNT): induction of DNA damage in plant and mammalian cells, J. Hazard. Mater. 197 (2011) 327–336.
[77] A.M. Tavares, H. Louro, S. Antunes, S. Quarre, S. Simar, P.J. De Temmerman, E. Verleysen, J. Mast, K.A. Jensen, H. Norppa, F. Nesslany, M.J. Silva, Genotoxicity evaluation of nanosized titanium dioxide, synthetic amorphous silica and multi-walled carbon nanotubes in human lymphocytes, Toxicol. In Vitro 28 (2014) 60–69.
[78] K.J. Siegrist, S.H. Reynolds, M.L. Kashon, D.T. Lowry, C. Dong, A.F. Hubbs, S.H. Young, J.L. Salisbury, D.W. Porter, S.A. Benkovic, M. McCawley, M.J. Keane, J.T. Mastovich, K.L. Bunker, L.G. Cena, M.C. Sparrow, J.L. Sturgeon, C.Z. Dinu, L.M. Sargent, Genotoxicity of multi-walled carbon nanotubes at occupationally relevant doses, Part. Fibre Toxicol. 11 (2014) 1–15.
[79] H.K. Lindberg, G.C. Falck, R. Singh, S. Suhonen, H. Jarventaus, E. Vanhala, J. Catalan, P.B. Farmer, K.M. Savolainen, H. Norppa, Genotoxicity of short single-wall and multi-wall carbon nanotubes in human bronchial epithelial and mesothelial cells in vitro, Toxicology 313 (2013) 24–37.
[80] M.T. Smith, K.Z. Guyton, C.F. Gibbons, J.M. Fritz, C.J. Portier, I. Rusyn, D.M. DeMarini, J.C. Caldwell, R.J. Kavlock, P.F. Lambert, S.S. Hecht, J.R. Bucher, B.W. Stewart, R.A. Baan, V.J. Cogliano, K. Straif, Key characteristics of carcinogens as a basis for organizing data on mechanisms of carcinogenesis, Environ. Health Perspect. 124 (2016) 713–721.
[81] L.G. Hernandez, H. van Steeg, M. Luijten, J. van Benthem, Mechanisms of non-genotoxic carcinogens and importance of a weight of evidence approach, Mutat. Res. 682 (2009) 94–109.
[82] N.R. Jacobsen, P.A. White, J. Gingerich, P. Moller, A.T. Saber, G.R. Douglas, U. Vogel, H. Wallin, Mutation spectrum in FE1-MUTA(TM) Mouse lung epithelial cells exposed to nanoparticulate carbon black, Environ. Mol. Mutagen. 52 (2011) 331–337.
[83] N.R. Jacobsen, G. Pojana, P. White, P. Moller, C.A. Cohn, K.S. Korsholm, U. Vogel, A. Marcomini, S. Loft, H. Wallin, Genotoxicity, cytotoxicity, and reactive oxygen species induced by single-walled carbon nanotubes and C(60) fullerenes in the FE1-Mutatrade markMouse lung epithelial cells, Environ. Mol. Mutagen. 49 (2008) 476–487.
[84] Y. Cao, N.R. Jacobsen, P.H. Danielsen, A.G. Lenz, T. Stoeger, S. Loft, H. Wallin, M. Roursgaard, L. Mikkelsen, P. Moller, Vascular effects of multiwalled carbon nanotubes in dyslipidemic ApoE−/− mice and cultured endothelial cells, Toxicol. Sci. 138 (2014) 104–116.
[85] J.D. Amaral, J.M. Xavier, C.J. Steer, C.M. Rodrigues, The role of p53 in apoptosis, Discov. Med. 9 (2010) 145–152.
[86] P. Georgiev, F. Dahm, R. Graf, P.A. Clavien, Blocking the path to death: anti-apoptotic molecules in ischemia/reperfusion injury of the liver, Curr. Pharm. Des. 12 (2006) 2911–2921.
[87] M.A. Hollingsworth, B.J. Swanson, Mucins in cancer: protection and control of the cell surface, Nat. Rev. Cancer 4 (2004) 45–60.
[88] M. Komatsu, S. Jepson, M.E. Arango, C.A. Carothers Carraway, K.L. Carraway, Muc4/sialomucin complex, an intramembrane modulator of ErbB2/HER2/Neu, potentiates primary tumor growth and suppresses apoptosis in a xenotransplanted tumor, Oncogene 20 (2001) 461–470.
[89] M. Perrais, P. Pigny, M.C. Copin, J.P. Aubert, S. Van, I. Induction of MUC2 and MUC5AC mucins by factors of the epidermal growth factor (EGF) family is mediated by EGF receptor/Ras/Raf/extracellular signal-regulated kinase cascade and Sp1, J. Biol. Chem. 277 (2002) 32258–32267.
[90] C.J. Yu, P.C. Yang, C.T. Shun, Y.C. Lee, S.H. Kuo, K.T. Luh, Overexpression of MUC5 genes is associated with early post-operative metastasis in non-small-cell lung cancer, Int. J. Cancer 69 (1996) 457–465.
[91] H. Awaya, Y. Takeshima, M. Yamasaki, K. Inai, Expression of MUC1, MUC2, MUC5AC, and MUC6 in atypical adenomatous hyperplasia, bronchioloalveolar carcinoma, adenocarcinoma with mixed subtypes, and mucinous bronchioloalveolar carcinoma of the lung, Am. J. Clin. Pathol. 121 (2004) 644–653.
[92] D.W. Kufe, Mucins in cancer: function, prognosis and therapy, Nat. Rev. Cancer 9 (2009) 874–885.